Available online at www.sciencedirect.com
SCIENCE DIRECT
Catalysis Today 105 (2005) 183–205
CATALYSIS TODAY
www.elsevier.com/locate/cattod

Field electron and field ion microscopy studies of chemical wave propagation in oscillatory reactions on platinum group metals

V.V. Gorodetskii [a,*], V.I. Elokhin [a], J.W. Bakker [b], B.E. Nieuwenhuys [b]

[a] *Boreskov Institute of Catalysis, Pr. Ak. Lavrentieva 5, Novosibirsk 630090, Russia*
[b] *Leiden University, Surf. Science and Het. Catalysis, Einsteinweg 55, 2333 CC Leiden, The Netherlands*

Abstract

The present paper reviews investigations, concerning the reactions of $CO + O_2$, $H_2 + O_2$, $NO + H_2$ on Pt, Pd, Rh and Ir tip surfaces studied on an atomic level. The main goal of the study was to obtain more detailed information on the mechanism of spatio-temporal oscillations on nanoplane surfaces with the help of field electron microscopy (FEM) and field ion microscopy (FIM). Sharp tips in size up to several hundreds of Angstroms have been used to carry out in situ investigations of real dynamic surface processes where different crystallographic nanoplanes of the tip are simultaneously exposed to the reacting gas and for which it is possible to study the interaction and the coupling of adjacent planes. The sustained temporal oscillations are associated with the appearance of propagation waves, which are generated by coupling of oscillations on adjacent crystal planes. Three fundamentally different feedback mechanisms generating kinetic oscillations have been identified: periodic changes in surface structure (Pt tip: $CO + O_2$, $H_2 + O_2$), subsurface oxygen formation (Pd tip: $CO + O_2$) and a strongly non-linear interaction between adsorbed species (Rh and Ir tips: $NO + H_2$). Based on experimental results, a model for the carbon monoxide–oxygen reaction on Pt(1 0 0) and Pd(1 1 0) surfaces is proposed for mathematical Monte Carlo modeling.

Keywords: CO oxidation; H_2 oxidation; NO reduction; Pt; Pd; Rh; Ir; Tips; Chemical wave; Oscillations; Field electron microscopy; Field ion microscopy; Monte Carlo modeling

1. Introduction

The early work of Nicolis and Prigogine [1] on non-equilibrium thermodynamics initiated numerous studies on oscillating reaction systems far from equilibrium. In heterogeneously catalyzed surface reactions, far from thermodynamic equilibrium, new phenomena may develop, such as instabilities, oscillations, chemical waves or chaotic behaviour, as summarized in review articles [2–6]. The great interest in self-oscillatory phenomena in catalytic reactions on metal surfaces is, for a large part, caused by the possibility to perform the catalytic processes more efficiently using unsteady-state operation. The oscillation cycles of the different products may have different forms and surface phases with respect to each other; this can produce valuable information on the mechanism of such reactions.

The extensive studies of model reactions ($CO + O_2$, $CO + NO$, NO_x and H_2, etc.) have been stimulated by the relevance of these reactions to air pollution control [7]. The automotive catalyst is based on the precious metals, usually Pt, Rh or Pd. CO oxidation and NO_x reduction on noble metal surfaces are highly non-linear systems. Usually, these reactions are operated under conditions far from the thermodynamic equilibrium, where temporal and spatial organization becomes possible. As a consequence, hysteresis and bistability also are observed when the external control parameters of reaction (partial pressures, flow rates and temperature) are changed. Detailed information on the relevant processes that are combined with these oscillations was obtained from experimental investigations on well-defined single crystal surfaces. Mechanisms of oscillatory reactions such as CO oxidation, H_2 oxidation, $NO + CO$,

* Corresponding author. Fax: +7 3832 308056.
E-mail address: Gorodetsk@catalysis.ru (V.V. Gorodetskii).

0920-5861/$ – see front matter © 2005 Elsevier B.V. All rights reserved.
doi:10.1016/j.cattod.2005.03.082

$NO + H_2$ or $NO + NH_3$ reactions are connected with a periodic change in surface structure Pt(1 0 0)-hex $\Leftrightarrow$ (1 × 1), with subsurface oxygen formation (Pd(1 1 0): $O_{ads} \Leftrightarrow O_{sub}$) and a strongly non-linear interaction between adsorbed species [2–6]. In addition, at high pressures of reactants the kinetic oscillations could be explained via oxide or carbon models. The vacant site model is used for the description of kinetic oscillations in the $CO + NO$ and $NO + H_2$ reactions by considering "surface explosions" which occur repeatedly at regular intervals [6]. A common feature in all these mechanisms is the spontaneous periodical transitions of the metal from an inactive to a highly active state.

Different mesoscopic and microscopic analytical tools have been introduced and successfully applied to learn details about the reaction dynamics at metal surfaces [3–6,8,9]. On single crystal planes oscillatory behaviour has been detected by mass spectrometric measurements of the CO_2-production, by monitoring of the work-function changes of the CO- or O-covered surface, by photoemission electron microscopy (PEEM), low energy electron diffraction (LEED), low energy electron microscopy (LEEM) and mirror electron microscopy (MEM) [10–15]. During catalytic reactions the formation of the target pattern and the propagation of reaction-diffusion fronts were observed. The method of PEEM with a spatial resolution of ∼1 μm made it possible to discover in the early 1990s a new phenomenon: the formation of chemical waves at CO oxidation on the surfaces of Pt and Pd single crystals [2–4]. Inspired by these experimental results field electron microscopy (FEM) with the higher lateral resolution of ∼20 Å and field ion microscopy (FIM) with near-atomic resolution of ∼3–6 Å have been applied for investigation of the formation of chemical waves at CO oxidation and NO reduction on Pt and Rh tip surfaces [8,9,16]. Sharp tips in size up to several hundreds of Angstroms have been used to investigate in situ real dynamic surface processes where different crystallographic nanoplanes of the tip are simultaneously exposed to the reacting gas and for which it is possible to study the interaction and the coupling of adjacent planes [17]. Many of the oscillatory reactions detected on tips are examples of such interplay of the different surfaces present. FEM/FIM studies of oscillatory reactions have been realized with several types of reaction systems: $H_2 + O_2$ on Pt [17]; $CO + O_2$ on Pt [18–20] and Pd [21]; $NO_2 + H_2$ on Pt [22]; $NO + H_2$ on Pt [23,24], Ir [25,26] and Rh, $NO + NH_3$ on Rh [30]. These investigations demonstrate that the chemical waves on the tip surfaces nucleated at local nanoplanes. This interaction can obviously not be studied with large single crystals and is lost in the *black box* techniques of the macroscopic world of the supported catalyst. Real metal/support catalysts usually consist of nano-sized metal particles on which different crystal planes are exposed. Therefore, the reaction kinetics on a supported metal catalyst might be quite different as compared to that on single crystal surfaces, as a result of interplay between different nanoplanes present on small particles. These surfaces, with a crystallite size of 100–300 Å, are mainly formed by the densest (1 1 1), (1 0 0), (1 1 0) planes, which differ drastically towards the adsorption and oscillatory behaviour. The direct comparison of adsorption and catalytic properties of nanosized planes (supported metal particles, 30–300 Å), with those of sharp tips ($\sim 10^3$ Å) and extended single crystal surfaces (1 cm^2) gives the possibility to bridge the "material gap" between single crystal surfaces and small metal particles, and to establish the intrinsic interrelation of oscillatory reaction mechanism on these surfaces.

In the present contribution, we report the observation of oscillations and surface wave propagation in $H_2 + O_2$, $CO + O_2$, $NO + H_2$ reactions on Pd, Rh, Ir and Pt tips under low pressure conditions. Not only oscillatory behaviour of the reaction rate (temporal oscillations) but also chemical waves moving directly on the catalytic surface (spatial phenomena) can be observed. Visualization was made possible by the use and the development of two spatially resolving surface science techniques: FIM and FEM. Certainly, the FIM/FEM technique is much less conventional than the PEEM, but its unique capacity to view directly the atomic structure of metal surfaces gives it a rightful place in the study of, for example, surface phase transitions or faceting mechanisms during oscillatory behaviour.

Obvious questions related to the appearance of sustained spatiotemporal oscillations on FEM/FIM tips and such which will be discussed later, are: what is the nature of the moving waves; what sites are responsible for their initiation; is there any relation between these spatiotemporal waves observed with FEM/FIM on metal tips and those found with PEEM on macroscopic single crystal surfaces. Statistical lattice models [31] describing the oscillatory behaviour of the CO oxidation on Pt(1 0 0) and Pd(1 1 0) surfaces will be developed and analyzed.

2. Experimental techniques on an atomic scale

2.1. Experimental techniques in FEM and FIM

Experiments with field electron and field ion microscopes were performed in a UHV (ultrahigh vacuum) chamber (base pressure $<10^{-10}$ mbar), which was used simultaneously as a flow catalytic reactor, Fig. 1a. The most convenient method of tip preparation is the shaping of the end of a thin wire to a tapered cone by anodic electropolishing [32]. Depending on tip-radius preparation, different crystallographic surface planes may have linear dimensions of 50–200 Å. Details of the tip preparation and of the Pt-group metals cleaning procedures have been given elsewhere: Pt [9], Ir [23], Rh [27], Pd [33]. The catalyst was a Pt-emitter tip of small radius (∼680 Å), prepared from a spectroscopically pure Pt-wire (0.1 mm Ø), spot-welded to a tungsten-heating loop. The method for producing clean stable Pt tips, along with the experimental set-up has also

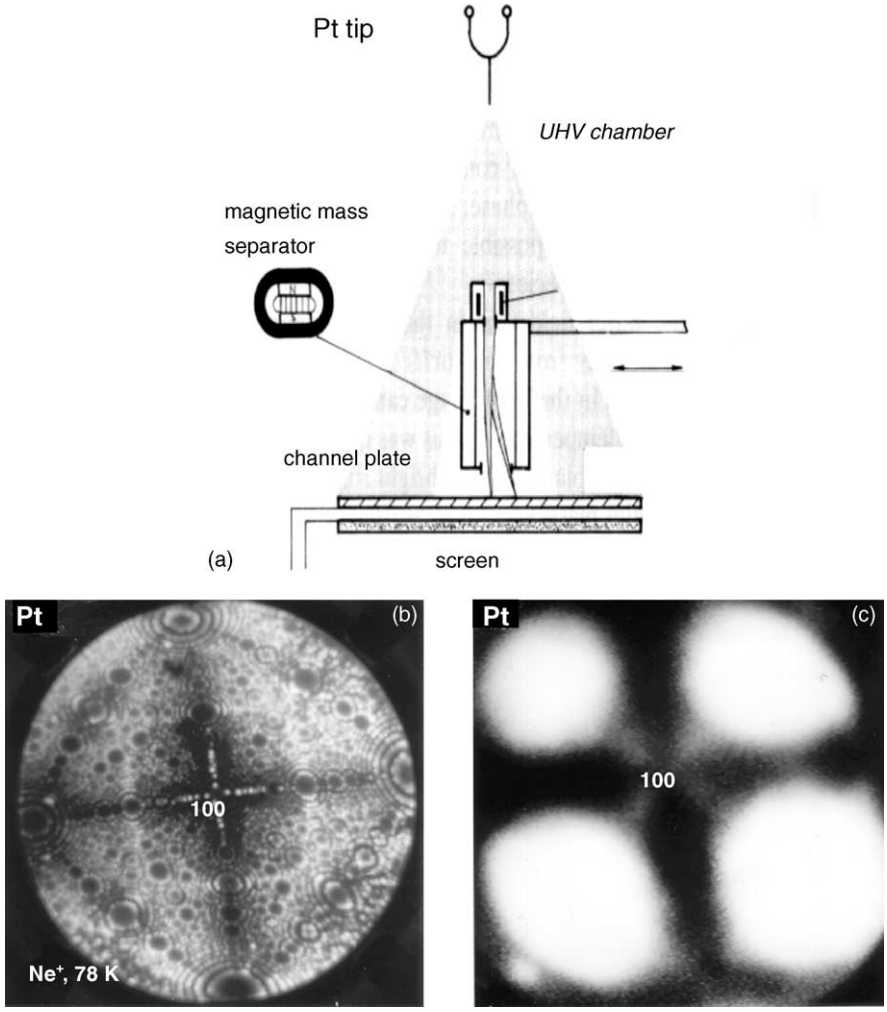

Fig. 1. (a) The UHV chamber for imaging surface waves during oscillations. Field ions in the FIM or field electrons in the FEM from the tip are impinging at the detector consisting of a high sensitivity channel plate and a screen. The images are recorded with a video camera. (b) FIM image of a Pt tip imaged with Ne^+ at 78 K; field evaporated at 16.5 kV; best image voltage at 15 kV, $P(Ne) = 2 \times 10^{-4}$ mbar; tip radius, $r = 680$ Å, $F \approx 4.2$ V/Å. (c) FEM-image of the same [0 0 1]-oriented Pt tip, ~1 kV; $F \approx 0.3$ V/Å [19].

been described elsewhere [9]. The Pt surface was cleaned by field evaporation and characterized with the field ion microscope by using Ne as an image gas at a field of ~3.5 V/Å (Fig. 1b). The resulting FEM image is shown in Fig. 1c. Another procedure for cleaning Pd tips uses thermal annealing to 1000 K at 10^{-10} mbar in several cycles and subsequent Xe-ion sputtering in the FEM regime in the presence of $P(Xe) \approx 10^{-3}$ mbar [33]. A digital field electron microscope has been used for Rh and Ir tip studies [34,35].

The field emission and field ionization microscopes were operated with low electron and ion currents (≈0.1 nA) to minimize gas collisions. The temperature at the tip could be controlled to within 1 K and was measured by means of a chromel/alumel thermocouple spot-welded to the metal loop near the tip. The reaction gases CO, NO, H_2 and O_2 of highest purity were introduced and measured with a quadrupole mass spectrometer. The FEM image and total field electron current were continuously monitored during the catalytic surface reaction at an oxygen partial pressure of $\approx 10^{-3}$ mbar and carbon monoxide partial pressure of $\approx 10^{-4}$ mbar. A double channel plate was used as an image amplifier of a small electron emission current (<1 nA), and a CCD camera with a time resolution of 40 ms recorded in situ the dynamic behaviour of the catalytic CO, H_2 oxidation and NO reduction reactions. It was demonstrated that at a pressure of up to $\approx 10^{-3}$ mbar, stable emission currents could be obtained and the sputtering processes seem to be completely negligible. The surface analysis of the Pt emitter is based on the fact that due to adsorption of NO, CO, H_2 and oxygen, local work function changes ($\Delta\Phi$) can be correlated with the total field electron current, as described before [36]. The field electron current (FEM) measures local properties of a surface with a lateral resolution of ~20 Å and magnification of $\sim 3 \times 10^5$. The in situ measurement of surface reactivity, which is combined with work-function alterations, concerns different surface orientations simultaneously. Electrostatic field effects at a field of ~0.4 V/Å during FEM investigations have not been observed in accordance with [37].

In FIM, instead of applying usual imaging gases (He, Ne, etc.) the reaction gas mixture itself is used to image the surface. As will be shown later the unexpected surface specificity in field ionization processes results in a new informative method display directly catalytically reacting surfaces in situ on the atomic scale. Chemical analysis of the surface processes involved in $H_2 + O_2$ and $CO + O_2$ oscillating reactions has been obtained by applying field- and laser-pulse desorption mass-spectrometry [38,39] or by analyzing the field ion current with mass spectrometric techniques [18]. In the first case, a surface analysis of adsorption layers is possible [39]. In the second case, ionized desorption products of the catalytic reaction are analyzed by mass spectrometry [18]. The electrostatic field strength for imaging the surface in these reactions by FIM was rather low, from $F \approx 1.0$ to 1.5 V/Å.

2.2. The imaging process of the catalytic surface reaction in the FEM

Field electron microscopy in its basic form is quite easy to understand. A negative voltage, V, of several kilovolts is applied to a metal tip. Upon increasing the field strength both the height and the width of the energy barrier decrease. Electrons are emitted into vacuum from the tip by tunneling through a potential barrier at the surface by the applied field and are accelerated towards a fluorescent screen, Fig. 1c. The resolution is limited to ~20 Å by the tangential velocity of the electrons in the free electron gas. The higher the applied voltage the higher the emission current, I, will be. Work function changes have been determined from the current–voltage characteristics by using the Fowler–Nordheim equation [40]:

$$I = AV^2 \exp\left(\frac{-B\Phi^{3/2}}{V}\right) \quad (1)$$

where I is the current measured at the fluorescent screen, V the applied voltage at the tip, A and B are constants and Φ is the work function. The slopes from the plots of $\log(I/V^2)$ versus $1/V$, α_{ads} and α_0 for the covered and clean tip, respectively, can be used to determine the work function Φ_{ads} using:

$$\Phi_{ads} = \Phi_0 \left(\frac{\alpha_{ads}}{\alpha_0}\right)^{-2/3} \quad (2)$$

where Φ_0 is the work function of the clean surface. The Φ_0 value used in this study for Pt is 5.3 eV. The value $\Delta\Phi$ is often used and is given by subtracting Φ_{ads} from Φ_0.

This method is however not effective when trying to measure a rapidly changing work function. In that case, a simplified version of the Fowler–Nordheim equation is used:

$$\frac{\Delta\Phi}{\Phi_0} = \left(\frac{1 + \Delta V}{V_0}\right)^{2/3} - 1 \quad (3)$$

Although, it is still necessary to confirm that this equation represents the true situation. This methodology has been described in detail, see [41].

2.3. The imaging process of the catalytic surface reaction in the FIM

Mainly noble gases (He, Ne) have been used in the field ion microscope to produce atomically resolved surface sites of the field emitter tip [32]. The high electric field strength is required for imaging of Pt tip surface in Ne ions. When the applied field at the tip approaches $F \sim 3.5$ V/Å for ionization of Ne (ionization potential 21.5 eV), neon atoms at the surface may loss a valence electron to the metal by tunneling. Field-ion energy distributions demonstrate that Ne atoms are ionized in a volume of space ~5 Å thick, and localized above the atoms of the tip surface. The positive ions will accelerate from the tip surface in a radial direction to the screen. At an imaging gas pressure of $P(\text{Ne}) = 2 \times 10^{-4}$ mbar, approximately up to $\sim 10^4$ ions s^{-1} are created above each protruding surface atom. This corresponds to an ion current of $\sim 10^{-14}$ A that demands amplification of the image with a high-sensitivity microchannel plate ion detector. The resolution of the FIM is determined by the spread in the kinetic energy of the imaging gas ions parallel to the tip surface, the spatial extent of the ionization zone, and diffraction effects of the ions. A high lateral resolution of ≈3 Å, is achieved at low temperatures by Ne imaging, Fig. 1b. It has been shown recently that chemically reacting molecules can also serve as imaging species [16,17,22,26] with a reduced resolution at a relatively low field strength ($F \approx 1.0$–1.5 V/Å).

2.3.1. Carbon monoxide oxidation

The gas mixture of CO and O_2, which reacts at the surface catalytically towards CO_2, serves at the same time as imaging gas in the field ionization process of the field ion microscope. The CO oxidation proceeds via a Langmuir–Hinshelwood reaction:

1. $CO_{gas} + * \leftrightarrow CO_{ads}$;
2. $O_{2gas} + 2* \rightarrow 2O_{ads}$;
3. $CO_{ads} + O_{ads} \rightarrow CO_{2gas} + 2*$;

where oxygen needs two adjacent empty sites for the dissociative adsorption. It is well known that during kinetic oscillations in CO oxidation on Pt(1 1 0) ($T = 427$ K, $P(\text{CO}) = 3 \times 10^{-5}$ mbar, $P(O_2) = 3.2 \times 10^{-4}$ mbar) PEEM images shows the development of adsorption islands formed for CO_{ads} as well as for O_{ads}, whereas CO_2 immediately desorbs at reaction temperatures [2–4]. The catalytic reactivity is high at the borderline between O_{ads} and CO_{ads} islands and, minor in O_{ads} islands [18]. Within the CO_{ads} islands O_2 adsorption is inhibited and, therefore, the catalytic reaction is poisoned.

FIM observations demonstrated that oxygen could be used as the imaging gas in the catalytic CO oxidation on Pt

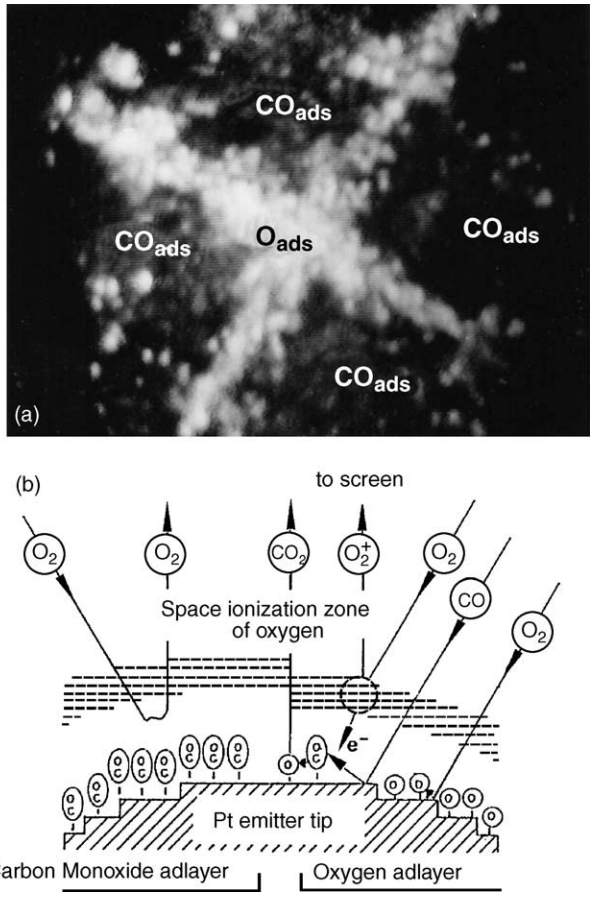

Fig. 2. (a) FIM image of a Pt tip taken at $T = 365$ K, $P(CO) = 5 \times 10^{-5}$ mbar, $P(O_2) = 5 \times 10^{-4}$ mbar; $F \approx 1.5$ V/Å. O_{ads} sites {(0 0 1) plane and [0 0 1] vicinals} re-imaged in the form of bright spots, while CO_{ads} sites {1 1 1 planes and surroundings} remain dark. (b) Field ionization process at a Pt-field emitter tip partially covered with CO_{ads} and O_{ads}. Oxygen molecules are field ionized only at surface sites that are covered with O_{ads} [42].

[16]. Thus, with a lateral resolution of ≈5 Å, the different adsorption sites for O_{ads} and CO_{ads} could be distinguished. The appearance and the disappearance of these sites in FIM gave an image of the Pt surface during the catalytic reaction. The field ionization process is illustrated in Fig. 2. The ionization potentials (I) of the involved reactant and product gases have different values: I_{O_2} (12.06 eV) < I_{CO_2}(13.76 eV) < I_{CO} (14.01 eV). Thus, with increasing field strength in the beginning of a field ionization process the oxygen molecular ions will be formed first. Adsorption layers furthermore influence the field ionization probability of oxygen. Experimental observations strongly suggest that O_{ads} sites are imaged by O_2^+ ions in the form of bright spots ($O_2 + O_{ads} \xrightarrow{field} O_2^+ + O_{ads} + e_{Me}^-$), while CO_{ads} sites remain dark [20,42]. The minimum ionization distance X_c for imaging gas particle, as given by:

$$X_c \approx \frac{I - \Phi}{F} \quad (4)$$

(F is the field strength in V/Å) is smaller for the O_{ads} sites ($X_c \approx 3.6$ Å) than for the CO_{ads} sites ($X_c \approx 4.0$ Å). The work function (Φ) of Pt surfaces is increased after CO adsorption ($\Delta\Phi \approx 0.7$ eV) and even more after adsorption of oxygen ($\Delta\Phi \approx 1.1$ eV). The applied field strength of $F = 1.5$ V/Å is just sufficient for field ionization of molecular oxygen at O_{ads} sites.

The high brightness imaging of oxygen-covered Pt tip surfaces using molecular oxygen as an imaging gas has been explained by a tunneling resonance state enhancing the field ionization rate of O_2^+ formation [43]. In spite of the fact that the critical distance of field ionization is quite far from O_{ads}/Pt surface, the wave function overlap of the participating highest occupied molecular orbital (HOMO) of O_2 and the lowest unoccupied state in the d-band of the surface is still substantial. This is not the case on the clean surface or CO-covered Pt surfaces. The brightness of the O_2^+ images of O-covered surfaces is the result of a resonance between the $2\pi_\alpha$ HOMO and the Pt–O-2p lowest unoccupied molecular orbital (LUMO) [43]. Thus, resonant field ionization is the perfect tool to image the oxygen-covered surfaces in ''titration reaction'' (Fig. 3) and in chemical waves (Fig. 7).

The surface plane specificity of the ''titration reaction'' of $O_{2gas} + CO_{ads} \rightarrow CO_{2gas} + O_{ads}$ is illustrated by FIM images in Fig. 3. In Fig. 3a, where the Miller indices are given, the Pt tip surface is initially covered with CO_{ads} and cannot be imaged. At a certain time, $\tau = 0$, O_{2gas} is added and the titration reaction starts on the {0 1 1} planes where the O_{ads} population is slowly increasing (b–f) to the moment when the (0 0 1) planes are quickly filled with O_{ads} (g). Finally, after a long period of time, the {1 1 1} planes are also covered with O_{ads} (h–i). Induction times (τ_i) and the rates of wave fronts propagation (Å s^{-1}) could be obtained from these experiments for the different planes. A maximum induction time is found for Pt(1 1 1), namely $\tau_i \sim 275$ s, and the rates of wave front propagation range from 0.8 Å s^{-1} (Pt(1 1 1)) to 500 Å s^{-1} (Pt(1 0 0)). A summary of the obtained values for the induction times and rates of wave front propagation are given in Table 1.

The titration reaction of precovered CO_{ads} with oxygen adsorbing from the gas phase displays a pronounced anisotropy. The slower motion of the wave front on high index planes is governed by a diffusion process and follows has a square root dependency as described by Fick's law. The diffusion coefficient of the wave front propagation, derived from the mean square displacement $\Delta r^2 = 4D\tau$, reaches a value of $D \approx 1.5 \times 10^3$ Å^2 s^{-1} which is nearly an order of magnitude smaller than the diffusion coefficient of CO on Pt at these conditions [42]. While oxygen atoms are rather immobile species on a platinum surface at 300 K, we have realized that CO_{ads} molecules diffuse in the opposite direction of the wave front propagation. The reaction towards CO_2 at the wave front forms empty sites that are occupied by the dissociating O_2 molecules. The propagation of the wave front therefore is partially ''eaten up'' by the reaction. The observed velocity of the wave front is

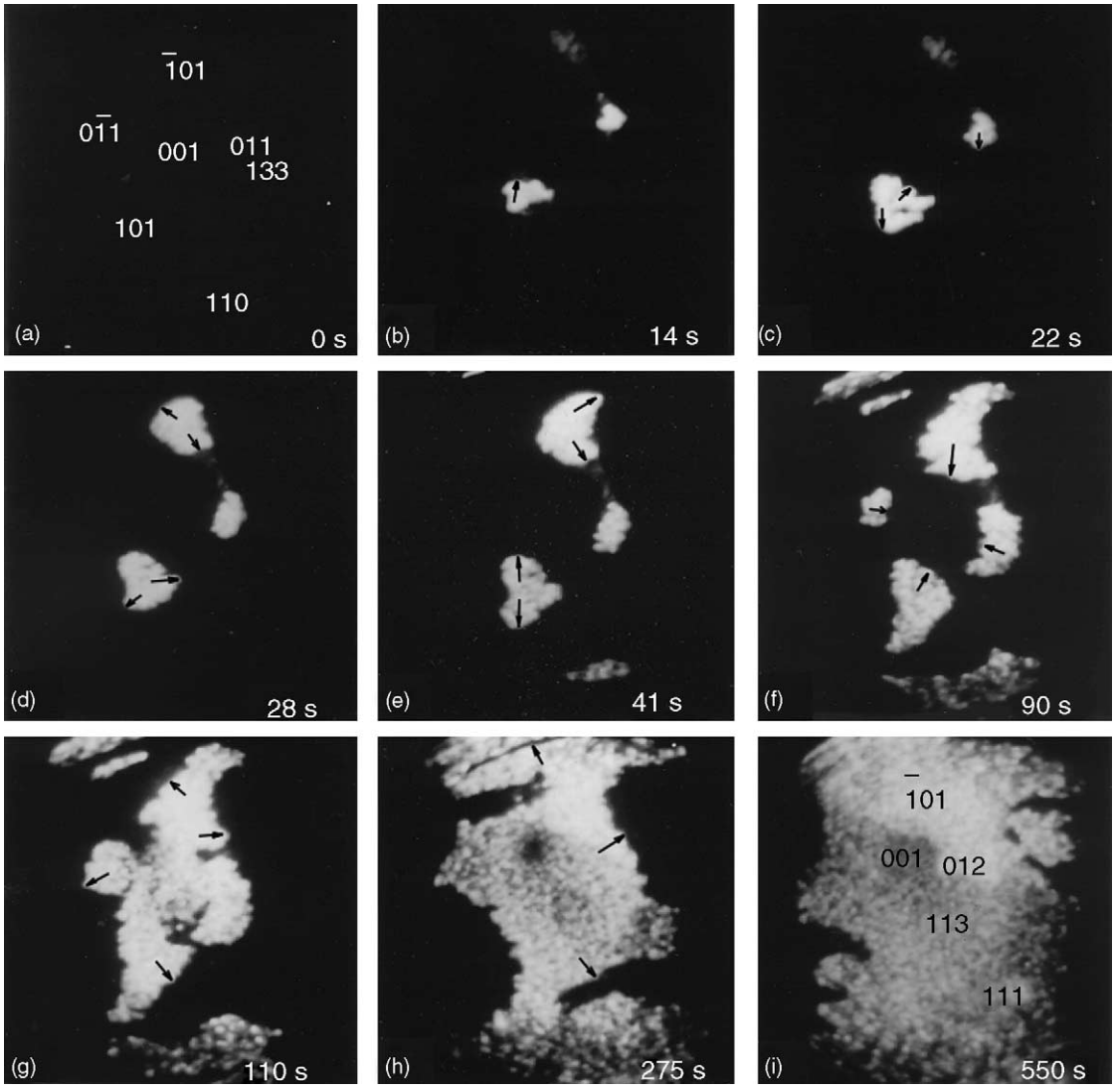

Fig. 3. FIM images measured during the titration reaction: $O_{2gas} + CO_{ads} \rightarrow CO_{2\ gas} + O_{ads}$ at 300 K. (a) Surface of a Pt tip precovered with CO_{ads} at $P(CO) = 5 \times 10^{-5}$ mbar, at $\tau = 0$. CO_{gas} pressure was removed and $P(O_2) = 5 \times 10^{-4}$ mbar introduced. (b) $\tau = 14$ s after the start of the titration reaction, adsorbed atoms O_{ads} are imaged as bright regions, residual $P(CO) = 1 \times 10^{-7}$ mbar. (c) 22 s; (d) 28 s; (e) 41 s; (f) 90 s; (g) 110 s; (h) 275 (s); (i) 550 s; $F \approx 1.5$ V/Å [42].

determined by the difference of two rates, namely the diffusion rate of CO_{ads} toward the CO_{ads}-layer and the CO_2 production rate at the phase boundary.

2.3.2. Hydrogen oxidation

The imaging situation for H_2 oxidation on Pt is even more dramatic because the product molecule of the catalytic reaction, H_2O, acts directly as an imaging gas [17,44]. Molecular water has an ionization potential of $I_{H_2O} = 12.60$ eV in the reaction gas mixture where $I_{O_2} = 12.06$ eV and $I_{H_2} = 15.42$ eV. At 300 K, H_2O, the reaction product of H_2 oxidation, desorbs immediately, with a very short residence time. It could be shown by mass spectrometry that in this reaction H_2O^+ (and H_3O^+) ions are the main ionic species that serve as the imaging gas in the FIM, thus indicating the site of the product formation [39]. It allows imaging of the active site of the catalyst surface in situ and in real time.

Table 1
The reaction specificity of different single crystal planes of a Pt tip during the titration reaction of a CO_{ads} layer with O_2 gas at $T = 300$ K and $P(O_2) = 5 \times 10^{-4}$ mbar

Planes Pt {*hkl*}	0 1 1	0 1 2	0 0 1	1 1 3	1 1 1
The induction time (s)	0	1	80	81	260
The rate of front propagation (Å s^{-1})	15	8	500	6	0.8

Following the literature data, water molecules are formed through a sequence of six reaction steps (in field-free conditions) [45]:

1. $H_{2gas} + 2^* \leftrightarrow 2H_{ads}$;
2. $O_{2gas} + 2^* \rightarrow 2O_{ads}$;
3. $O_{ads} + H_{ads} \rightarrow OH_{ads} + ^*$;
4. $2OH_{ads} \rightarrow O_{ads} + H_2O_{ads}$;
5. $2H_{ads} + O_{ads} \rightarrow H_2O_{ads} + 2^*$;
6. $H_2O_{ads} \rightarrow H_2O_{gas} + ^*$;

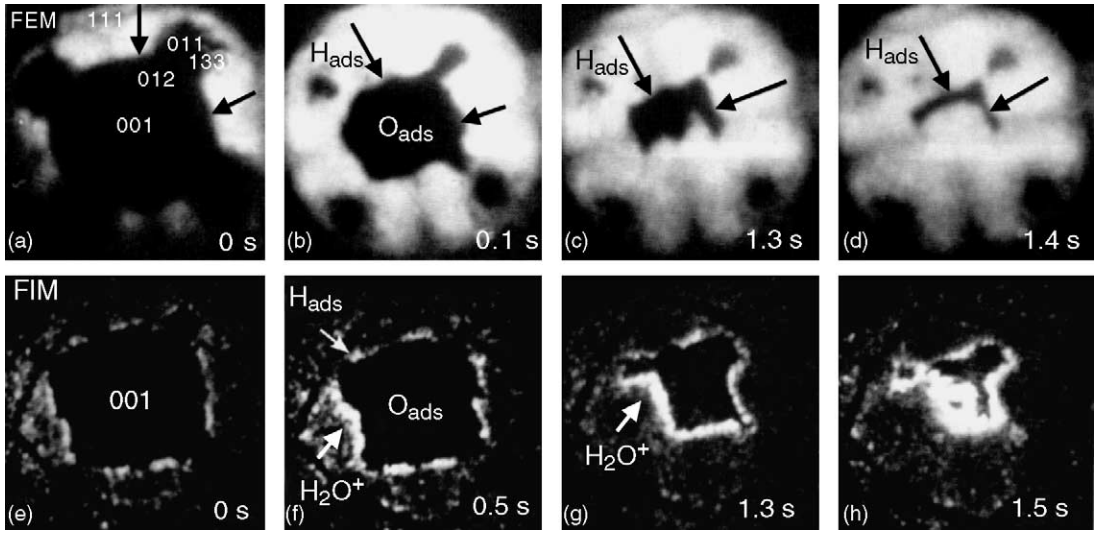

Fig. 4. FEM images (a–d) and FIM images (e–h) of a Pt tip (radius 1800 Å) during the titration reaction of O_{ads} with hydrogen at $P(H_2) = 4.6 \times 10^{-7}$ mbar, $T = 395$ K. In FEM images, the disappearance of the O_{ads} layer (black) is characterized by the formation of the H_{ads} layer (white); time values: (a) 0 s, (b) 1.0 s, (c) 1.3 s, (d) 1.4 s. In FIM images, a bright reaction front is imaged by the product ions (H_2O^+ and H_3O^+). It is moving into the following direction {1 3 3}, {1 1 1} → {0 1 2} → (0 0 1); time values: (e) 0 s, (f) 0.5 s, (g) 1.3 s, (h) 1.5 s [44].

Fig. 4 presents the images of the catalytic titration reaction $H_{2gas} + O_{ads} \rightarrow H_2O_{gas} + H_{ads}$. As can be seen from this figure the brighter front is produced by H_2O^+ ions being formed near the tip surface ($X_c \approx 4$ Å) from the desorbing reaction product ($H_2O_{gas} \longrightarrow^{field} H_2O^+_{gas} + e^-_{Me}$). Hence, in a unique fashion the temporarily catalytically active sites could be identified. It should be emphasized that the applied electrostatic field strength of $F \approx 1.5$ V/Å did not noticeably influence the kinetics of the H_2/O_2/Pt system [46]. In fact, reversing the polarity of the electric field did not affect the propagation velocities of chemical waves during the titration reaction of O_{ads} with hydrogen studied by FEM (negative field, $F \approx 0.4$ V/Å) and FIM (positive field, $F \approx 1.5$ V/Å). Fig. 4 illustrates the imaging process of the H_2 oxidation on a [0 0 1]-oriented Pt tip. Here the surface is first saturated with oxygen, O_{ads}, which then reacts with hydrogen from the gas phase in the titration reaction. In Fig. 4a–d the sequence of FEM images shows the dark O_{ads} layer (high work function values, $\Delta\Phi \approx 1.1$ eV) being transformed into a bright H_{ads} layer (low work function values, $\Delta\Phi \approx 0.2$ eV) via a reaction front in a face-specific reaction sequence starting (at $\tau = 0$) on the peripheric {1 1 1} planes and ending (after 1.4 s) on the (0 0 1) apex plane. The same titration reaction has also been studied by FIM (Fig. 4e–h). A bright reaction front is imaged here by the product ions (H_2O^+ and H_3O^+). Formation of H_3O^+ can occur during a field-induced surface reaction for a protonation pathway involving H_{ads} and H_2O_{ads}: $H_{ads} + H_2O_{ads} \longrightarrow^{field} H_3O^+_{gas} + e^-_{Me} + 2*$ [39,46].

2.3.3. Electrostatic field effect

The in situ imaging process of catalytic reactions differs considerably from the field ionization process of Ne, which generates the well-resolved Pt atomic surface structure in Fig. 1. Three reasons may explain the rather blurred FIM images of the catalytic processes: (i) the sharp images of Fig. 1 can be obtained only at cryogenic temperatures enabling an effective accommodation of the image gas; (ii) reaction products like H_2O may still carry a fraction of the reaction enthalpy as excess of lateral momentum, which leads to a decreasing resolution; (iii) fast surface diffusion processes may be involved before the formation of the imaging ions.

One of the major problems discussed in imaging surfaces by field electron and field ion microscopy concerns the influence of electric fields on chemical reactivity [47]. High electrostatic fields may be expected to disturb catalytic surface processes to such an extent that, other than normal catalytic reactions, ‘‘field-induced reactions’’ are observed. It should be mentioned that the physical processes that underlie the imaging of the $CO + O_2$ and the $H_2 + O_2$ reactions in FIM are quite different. For the former reaction O_2 is ionized by a field ionization process, i.e. an electron tunneling into the emitter. Thus, O_{2gas} – as imaging gas – preferentially shows oxygen adsorption sites. It is well known for other systems, for instance the behaviour of the NO molecules in high electric fields [47], that bond energies and molecular orientations are field-dependent and electrostatic fields can cause bond fission. We did not find an indication of these effects when O_2 was used as imaging gas to image the $CO + O_2$ reaction on Pt [16], where the electrostatic field in FIM is approximately two times higher than in FEM. It was suggested that due to field-compression the nominal pressure ranges for the oscillation regions are lower by a factor of 3 [16] as compared to studies on extended single crystal surfaces [48]. However, it should be noted that this effect could also be explained in terms of a field-induced enhancement of the binding energy of CO and

O_2 adsorbed on Pt tip surfaces [37,49]. For the $H_2 + O_2$ reaction the situation may be more complicated since the applied electric field introduces new reaction channels. In the latter case, a field-induced proton transfer of adsorbed hydrogen, H_{ads}, leads to the formation of hydronium ions H_3O^+.

3. Chemical waves in catalytic CO oxidation

3.1. Phase transitions of Pt(1 0 0)-hex ↔ 1 × 1: Pt tip experiments and modelling

We will first consider the CO oxidation on single crystal surfaces in order to discuss the benefits of microscopic techniques, such as FEM and FIM, for understanding the details of the reaction mechanisms involved during oscillatory behaviour. It is well known that the Langmuir–Hinshelwood mechanism can be used to describe the CO oxidation reaction on platinum group metals. A large number of studies have been published for the CO oxidation reaction on Pt(1 0 0), (1 1 0), (2 1 0) and Pd(1 1 0) single crystal surfaces where isothermal oscillations have been observed [2–5]. The Pt(1 1 1) surface does not show oscillations under UHV conditions. In order to explain the occurrence of kinetic oscillations a proper reaction mechanism has to be identified. It was demonstrated that the mechanism of kinetic oscillations during CO oxidation on a Pt(1 0 0) single crystal surface is connected with the surface reconstruction (Pt(1 0 0)-(hex) ↔ (1 × 1)) induced by CO adsorption [50]. From studies on other single crystal planes the region of external controlling parameters for which kinetic oscillations occur during CO oxidation were identified and this information serves as guidelines for the present investigations.

Some general questions have to be raised in this context:

(1) What minimum dimensions of the surface are required for observation of the reaction waves or other non-linear collective phenomena?
(2) How does the interplay of various adjacent nano-planes with different properties such as sticking, and diffusion coefficients, adsorption energies, etc., influences the oscillatory regimes?

3.1.1. Pt tip: FEM

As shown in an earlier study by Lim et al. [48], the existence of monostable and bistable regions as well as the oscillating regime can be evaluated with the help of FEM, and displayed in a kinetic phase diagram. Such a diagram has been established by us for the Pt(1 0 0) nanoplanes (∼200 Å dimension) on a Pt tip at 340 K (Fig. 5A) [18]. The diagram corresponds to the transitions from O/Pt(1 0 0) nanoplane presented in Fig. 5B-c to CO/Pt(1 0 0) one, Fig. 5B-e. This diagram coincides well with that for an extended Pt(1 0 0) single crystal surface, obtained at a much higher (440–520 K) temperature range [50].

Fig. 5B represents a typical sequence of FEM images for (1 0 0) nanoplanes obtained when a Pt tip with [1 0 0]-orientation is exposed to a gas mixture of $P(O_2) = 4 \times 10^{-4}$ mbar and $P(CO) = 8 \times 10^{-6}$ mbar at 340 K [18]. Oscillations are detected with emission current amplitudes ranging from O_{ads} (low current) to CO_{ads} (high current) layers and a periodicity of 27 s. The difference of the work function ($\Delta\Phi$) between O_{ads} and CO_{ads} of ∼0.4 eV is connected with a change in the electron current. Since the work function value is higher for a chemisorbed oxygen layer ($\Delta\Phi = 1.1$ eV) than that for a CO_{ads} layer ($\Delta\Phi = 0.7$ eV) [9], the relative surface brightness is dark for O_{ads}, grey for CO_{ads} and bright for unoccupied clean

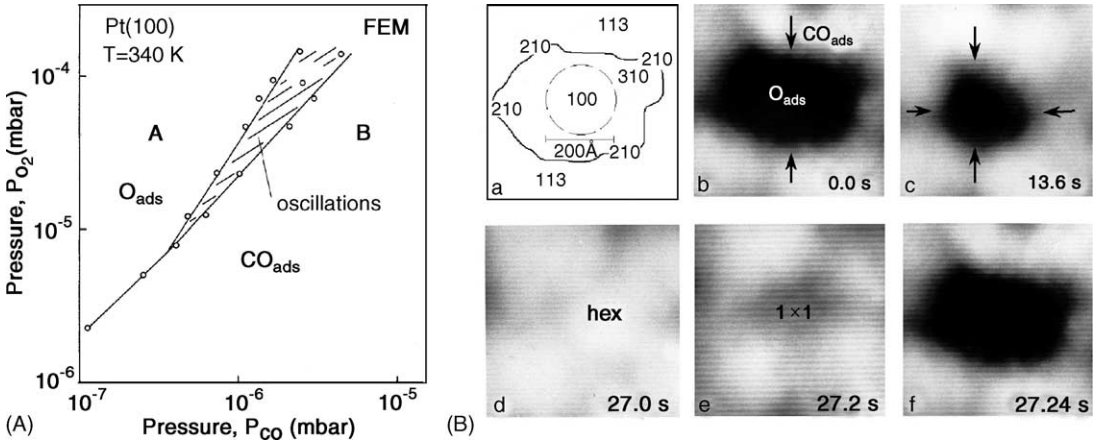

Fig. 5. (A) Phase diagram for CO oxidation on the (1 0 0) nanoplane of a Pt tip obtained at 340 K. The active O_{ads} layer (region A) and inactive CO_{ads} layer (region B), are separated by the indicated lines. The dashed region is the region of oscillatory behaviour. (B) Magnified view of a sequence of FEM images obtained along the (1 0 0) plane of a Pt tip during one oscillating cycle at 340 K and $P(CO) = 2.3 \times 10^{-6}$ mbar and $P(O_2) = 4 \times 10^{-4}$ mbar partial pressures. (a) Stereographic projection of a Pt[1 0 0]-oriented tip; (b) $\tau = 0$, the (1 0 0) plane is covered by O_{ads}; (c) after 13.6 s, the O_{ads} layer shrinks due to a slow reaction; (d) after 27.0 s, the very bright image indicates a clean and reconstructed (1 0 0)-hex surface; (e) $\tau = 27.2$ s, a small CO_{ads} coverage remains and the reconstruction is lifted; (f) restoration of the O_{ads} layer and the same condition as (b) [18].

surface sites. From earlier work [51], we have proposed that the ''clean-off'' reaction initiates the phase transition of the Pt(1 0 0)-(1 × 1) structure to the Pt(1 0 0)-(hex) structure. The ''clean-off'' reaction mechanism that takes place on the (1 0 0) nanoplanes at 340 K is illustrated in Fig. 5B. A view of the (1 0 0) plane (∼200 Å dimension) is shown where the O_{ads}-precovered surface ($P(O_2)$ kept constant at 4×10^{-4} mbar) is imaged during the reaction with additionally admitted CO ($P(CO) = 2.3 \times 10^{-6}$ mbar). At the beginning of the cycle, panel (b), the unreconstructed Pt(1 0 0)-(1 × 1) surface is completely covered with an O_{ads} island (shown as a dark patch). That island slowly reacts with CO_{ads}, and this process results in a gradual shrinkage of the O_{ads} layer, panel (c), until a very fast catalytic surface process (the ''clean-off'' reaction) removes the CO_{ads} layer. At that moment the clean unstable (1 × 1) surface suddenly reconstructs to the (hex) structure [51], creating an unoccupied clean Pt(1 0 0)-hex surface, panel (d), with high local electron emission current (hence the bright picture). The small (10^{-3}) sticking coefficient of oxygen on this surface, keeps this reconstructed plane free from O_{ads} until, at a certain local CO coverage, the reconstruction is lifted again, and the (1 × 1) structure is returned, panel (e). This is accompanied by an increase in oxygen sticking coefficient, from $\approx 10^{-3}$ (hex) to $\approx 10^{-1}$ (1 × 1) that induces a transition from a catalytically inactive state into an active surface for CO oxidation. Subsequently, due to a very fast reaction and oxygen adsorption (f) (within one video frame $\Delta t \approx 40$ ms), the initial state of O_{ads}-covered surface is regained (b). The details of the oscillatory behaviour strongly depend on the external control parameters, i.e., the selected temperature and partial pressures. For $T = 478$ K, the reaction/diffusion fronts propagate with a velocity of 5000 Å s^{-1} [9]. Rates of the fronts propagation having the same order of magnitude (∼3 μm s^{-1}) have been found previously on Pt(1 1 0) surfaces at 485 K during PEEM experiments [52]. Qualitatively similar results were also obtained for the Pt(1 0 0) crystal surface[53].

3.1.2. Pt tip: FIM

The results obtained by FEM reported before, showed that the field electron current could be used to characterize the different stages of an oscillating cycle. For comparison the total field ion currents at 365 K are shown in Fig. 6. The comparison with the FEM results leads to the conclusion that always-high ion currents belong to the O_{ads} layer and low currents to the CO_{ads} layer. According to FIM data presented in Fig. 3 the O_2^+ ions are imaging only those surface sites that are covered with adsorbed oxygen and not those that are empty or are covered with CO_{ads}. The temporal variation of the total O_2^+-ion current is caused by a pronounced spatial distribution of local ion currents. The FIM patterns, which describe different stages during the oscillations, are illustrated in Fig. 7. The inactive planes (a) display dark surfaces (except some defects which remain bright during the whole cycle). Oxygen adsorption starts at sites in the

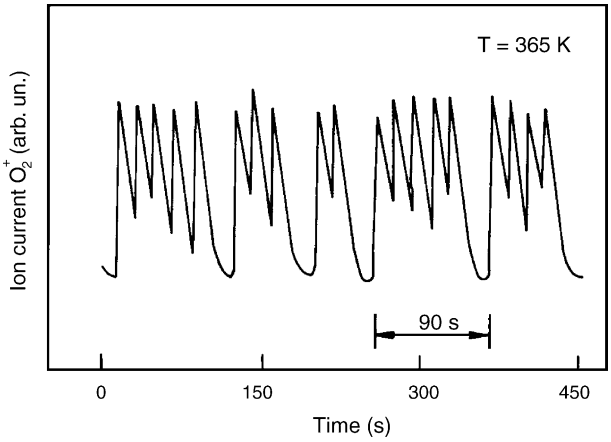

Fig. 6. Total O_2^+-ion currents during the oscillating CO oxidation at 365 K, $P(CO) = 5 \times 10^{-6}$ mbar, $P(O_2) = 5 \times 10^{-4}$ mbar [20].

{1 3 3} regions (b), than expanding the O_{ads} coverage from the {1 1 0} vicinity (c–e) to the central (0 0 1) plane (f). The {1 1 1} planes are still covered with CO_{ads} and remain in the same state for all experiments with this reaction on Pt. From these experiments – as described in detail in ref. [19] – the oscillations of the CO oxidation reaction rate are temperature-dependent, their frequencies change from $\sim 10^{-3}$ Hz at 330 K to $> 10^{-1}$ Hz at 500 K. Various kinds of mixed mode oscillations may occur at different temperatures. At temperatures $T > 445$ K morphological changes of the tip surface were detected.

Surprisingly, the FEM and FIM images have shown very sharp reaction fronts. Therefore the nature of the local reaction rates is of great interest. To obtain information about the chemical identity of the field emitted ions during the reaction, a mass-analysis by the atom-probe hole technique has been applied (Fig. 8a–c) [18,38]. For low partial pressure conditions ($P(O_2) = 1.5 \times 10^{-4}$ mbar, $P(CO) = 1 \times 10^{-5}$ mbar) and a reaction temperature of 450 K, the yield of CO_2 molecules (CO_2^+ ions) has shown a maximum intensity when the traveling reaction zone (oxygen wave front, Fig. 8b), with a space dimension of about 40 Å between O_{ads} and CO_{ads} layers, crosses the hole of an atom-probe. This CO_2^+ yield shows the low intensity on the CO_{ads}-side of the reaction and the high intensity on the O_{ads}-side of the reaction; the highest intensity is obtained when the reaction zone front passes, Fig. 8c. Possible mechanisms describing such a sharp reaction zone formation are based on a local transformation (hex) ↔ (1 × 1) of the Pt(1 0 0) single crystal surface and the appearance of empty sites. A clean hexagonally reconstructed boundary surrounds the oxygen island adsorbed on the 1 × 1 phase, as shown in Fig. 8b (thin bright line).

3.1.3. Modeling of oscillations and wave patterns

The mechanism of synchronization of local oscillators is one of the fundamental problems arising during the study of the oscillatory behaviour of heterogeneous catalytic reactions [5,17]. A statistical lattice model has been constructed

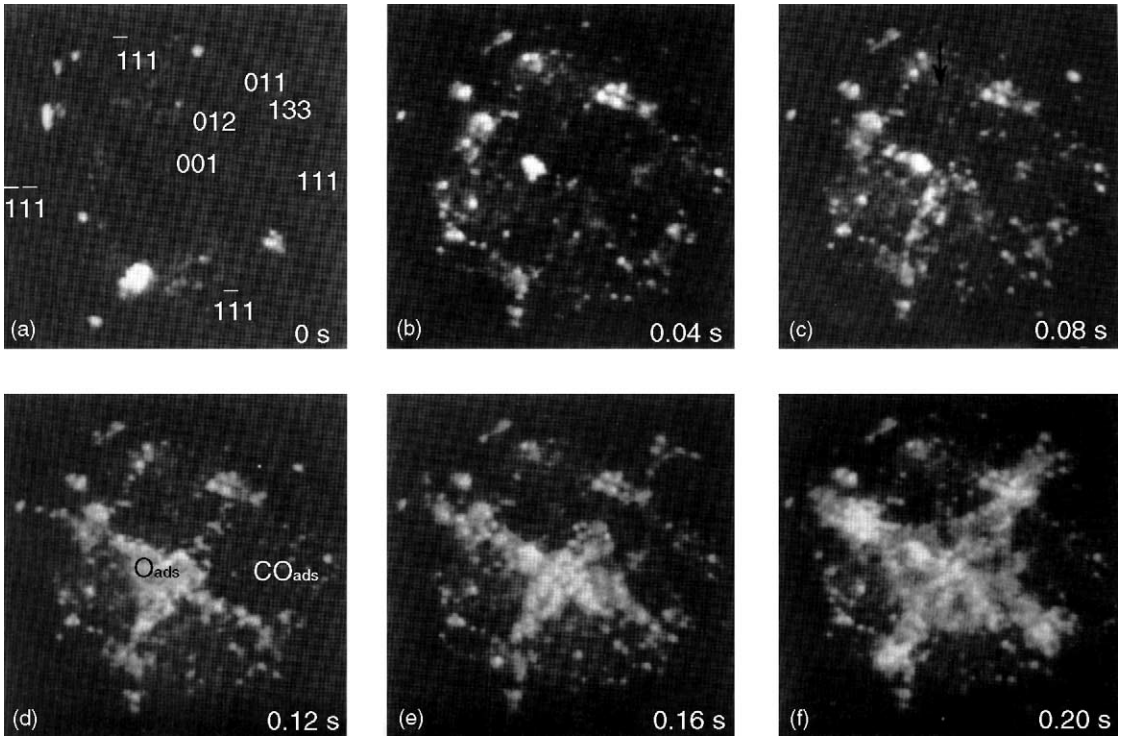

Fig. 7. FIM images characterizing different stages of the oscillatory behaviour presented in Fig. 4, details in the text [20].

for the $(CO + O_2)$/Pt(1 0 0) reaction which takes into account the change of the surface properties due to the adsorbate-induced reversible surface transformation hex ↔ 1×1 [54]. The model reproduces qualitatively the hysteresis and the oscillations in reaction rate, O_{ads}, CO_{ads} coverages, hex and 1×1 surface phases under conditions close to the experimental ones. Autowave processes accompany self-oscillations of the reaction rate.

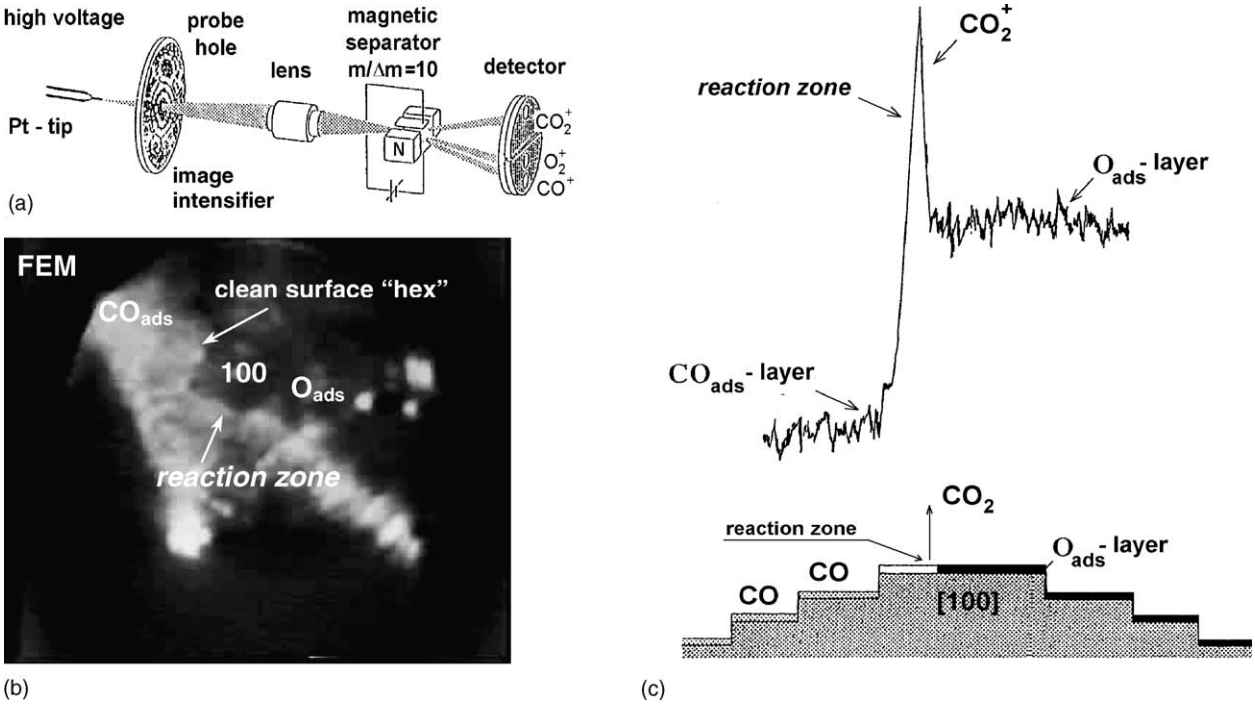

Fig. 8. Reaction/diffusion front monitored during $CO + O_2$ reaction on a [1 0 0]-oriented Pt field emitter. (a) Schematic presentation of the FIM mass-analysis implemented by the probe hole technique. (b) FEM image showing the surface structures of the oxygen island developed on the CO-precovered surface. The preadsorbed CO_{ads} layer in the presence of $P(CO) = 1 \times 10^{-5}$ mbar reacts with oxygen ($P(O_2) = 1.5 \times 10^{-4}$ mbar), producing a sharp O_{ads} wave front crossing the probe hole with a period of ∼100 ms. (c) CO_2^+ intensity on the CO_{ads}-side, O_{ads}-side of the reaction and on the reaction zone; $F \approx 2$ V/Å [18].

In general, in the case of single crystal and metal tip studies under reaction conditions of 10^{-5}–10^{-2} mbar, surface diffusion of the adsorbed species can be responsible for the synchronisation of local oscillators. In the early theoretical models of the (CO + O_2)/Pt(1 0 0) reactions, the rate of the hex → (1 × 1) transition was assumed to be linearly dependent on the local CO_{ads} coverage on the hex-phase (e.g., [55]). However, it has been shown recently by molecular beam studies that the (1 × 1)-CO island growth rate, and, therefore, the (1 × 1) phase, is governed by a strongly non-linear power law $\dot{\Theta}_{1\times1} \sim (\Theta_{CO}^{hex})^n$, where $\Theta_{1\times1}$ is a part of the surface transformed into the (1 × 1) phase, Θ_{CO}^{hex} is the CO coverage on the hex-phase, and $n \approx 4$ [56]. Subsequently this information was included in a new model accounting for the oscillatory behaviour of CO + O_2/Pt(1 0 0) reaction [57].

It has been found, that the Pt(1 0 0) surface switches reversibly from an inactive state (hex) into a highly active state (1 × 1) under conditions of CO + O_2 reaction rate self-oscillations. It has been established, that the low activity (hex) branch exhibited a low sticking coefficient for oxygen (S_{O_2}). In combination with the formation of CO islands, dissociation of the O_{2ads} is hindered. The high activity Pt(1 0 0)-1 × 1 surface has a high sticking coefficient (S_{O_2}) for oxygen and an increased population of atomic oxygen states. Three O_{ads} states have been observed by HREELS (high resolution electron energy loss spectroscopy). This is a result of the existence of the surface defect sites [58].

The detailed mechanism of this CO oxidation process may be considered as follows (see Scheme 1) [54]. (1) CO adsorption: it is suggested that CO molecules, in contrast to oxygen, have equal sticking probabilities on both $*_{hex}$ and $*_{1\times1}$ (* denotes the empty sites irrespective of its structure). (2 and 3) CO desorption: the rate coefficients for CO desorption on hex- and 1 × 1-phases differ widely (approximately by three-four orders of magnitude). (4) Structural phase transformation (hex) → (1 × 1): following ref. [56], it was supposed that the adsorption of four CO molecules on the 2 × 2 neighboring centres of the lattice would transform these centres (with some probability) into the (1 × 1) structure. (5) The reverse structural phase transition (1 × 1) → (hex). (6) Oxygen adsorption: oxygen adsorbs dissociatively only on the two neighbouring (1 × 1) centres. (7) CO_2 formation: adsorbed oxygen interacts equally with both CO_{ads}^{hex} and $CO_{ads}^{1\times1}$. (8) CO_{ads} diffusion: adsorbed carbon monoxide can diffuse via hopping from the occupied sites to the vacant nearest neighbour sites and the type of active centres remains the same. According to Scheme 1, the empty active centres $*_{1\times1}$ (initially covered by CO) appear due to the action of the stage 3 (but with very low probability of realization) or, predominantly, due to CO_{ads} diffusion process (stage 8). Along with stage 7, these processes represent the sources of empty active centres $*_{1\times1}$ required for the dissociative adsorption of oxygen.

(1) $CO + * \rightarrow CO_{ads}$

(2) $CO_{ads}^{hex} \rightarrow CO + *_{hex}$

(3) $CO_{ads}^{1\times1} \rightarrow CO + *_{1\times1}$

(4) (hex) → (1×1): $4CO_{ads} \rightarrow 4CO_{ads}^{1\times1}$

(5) (1×1) → (hex): $*_{1\times1} \rightarrow *_{hex}$

(6) $O_2 + 2*_{1\times1} \rightarrow 2O_{ads}^{1\times1}$

(7) $O_{ads}^{1\times1} + CO_{ads} \rightarrow CO_2 + *_{1\times1} + *$

(8) $CO_{ads} + * \rightarrow * + CO_{ads}$

Scheme 1.

Using this mechanism, the experimental results were simulated with the help of a Monte Carlo method. It was possible to reproduce both the oscillations observed for the rate of CO_2 formation and the appearance of surface waves on the Pt(1 0 0) single crystal plane [54].

The oscillations of the reaction rate, O_{ads} and CO_{ads} coverages, and hex and 1 × 1 surface phases are accompanied by surface wave propagation (Fig. 9). At the initial moment, the platinum surface is in the (hex) state and only CO adsorption (A) is allowed. Despite of the low rate of the (hex) → (1 × 1) transformation, the portion of the (1 × 1) rapidly grows. As a result of CO_{ads} diffusion, the sites for oxygen adsorption are formed. However, the value of $O_{(1\times1)}$ coverage is very low (Fig. 9A) due to the fast reaction with neighbouring CO_{ads} molecules. When the maximal value of $\theta(CO_{ads}) \sim 0.8$ is attained, the adsorbed layer largely consists of $CO_{(hex)}$ and $CO_{(1\times1)}$ (Fig. 9A), which is accompanied by a sharp decrease in the reaction rate. Fig. 9a shows that the rate of formation of CO_2 molecules in the CO_{ads} layer is low, but regions with an elevated concentration of vacant sites are available on the surface. In these regions, the $O_{(1\times1)}$ islands nucleate and propagate along the metal surface (Fig. 9B and C). Figures b and c also shows that the maximal intensity of CO_2 formation is observed in a narrow zone at the boundary of the growing O_{ads} phase and the CO_{ads} layer. The appearance of such a narrow reaction zone has been experimentally observed by the field ion probe-hole microscope with a resolution of ~5 Å, presented in Fig. 8. Inside the oxygen island, the rate of CO_2 formation has an intermediate value and the minimum value is obtained in the CO_{ads} layer. At the final stage of the oscillation cycle (Fig. 9D-d), the $\theta(CO_{ads})$ coverage increases due to CO adsorption on the vacant sites (both (hex) and (1 × 1)) with the further transition of the (1 × 1) phase into the (hex)-phase.

3.1.4. Summary

The results of FEM/FIM studies revealed that a CO-induced (hex) ↔ (1 × 1) phase transition, also observed on the macroscopic Pt(1 0 0) single crystal, is the driving force for the isothermal oscillations on the (1 0 0) plane of a microscopic grain. The reactive phase diagram for the (1 0 0) nanoplane of a Pt tip surface correlates with that for large Pt single crystals [48,50]. The FEM/FIM results on a Pt tip can be summarized as follows: (i) the kinetic oscillations of CO oxidation are face-specific processes and are observed for (1 0 0), (1 1 0) and (2 1 0), but not for (1 1 1), (1 1 2), (1 1 3) single crystal surfaces; (ii) chemical

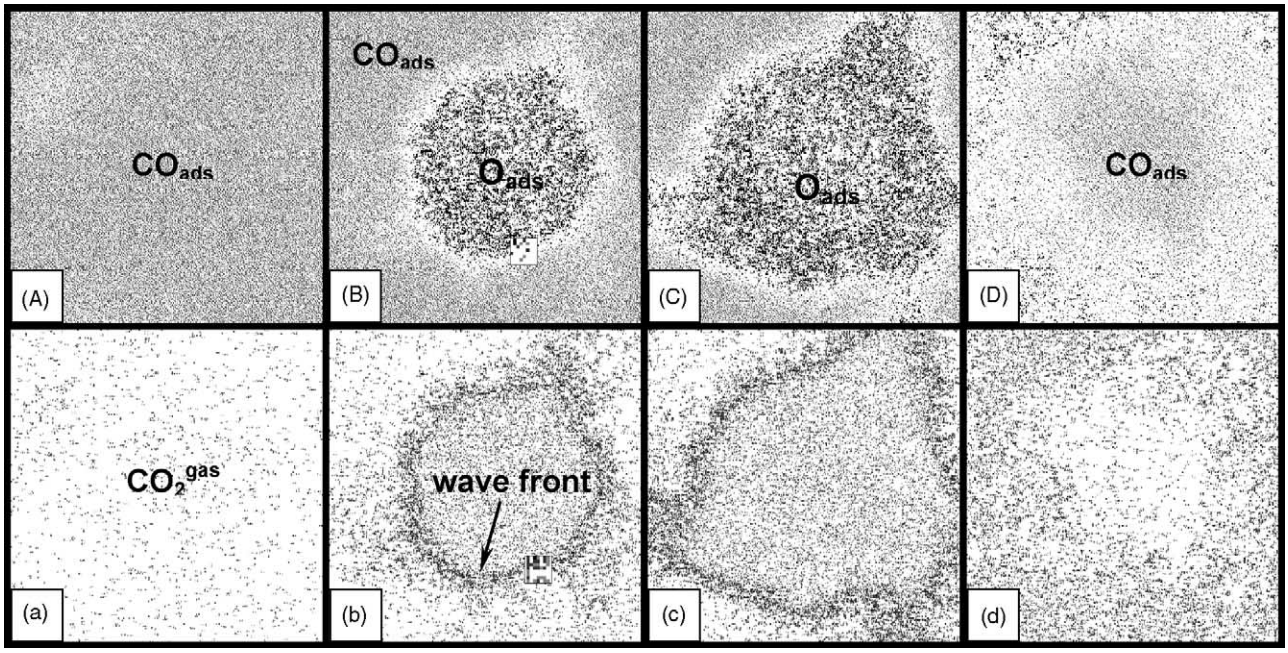

Fig. 9. Snapshots reflecting the distribution of adsorbates on the surface (A–D) and the distribution of the intensity of CO_2 formation (a–d) on (1 0 0) planes of a Pt tip during one oscillating cycle. On the A–D snapshots O_{ads} is painted in black, CO_{ads} in grey and empty Pt sites in white. On the a–d snapshots the intensity of the grey color reflects the value of the CO_2 production rate [54].

waves appear and propagate in phase with the self-sustained isothermal oscillations. Two spatially separated adlayers are formed under oscillating conditions. The CO_{ads}-covered layers are formed only on the {1 1 1}, {1 1 2}, {1 1 3} planes, whereas O_{ads}-covered areas are formed on the {1 0 0}, {2 1 0}, {1 1 0} planes. The observation of FEM patterns indicates that surface diffusion of reactants (CO_{ads}) seems to be the main coupling mechanism in the communication between different parts of a Pt tip surface. In the catalytic reaction CO_{ads} and O_{ads} wave fronts move alternately in opposite directions and display different velocities of propagation. A reaction zone of about 40 Å in width between the mobile waves of CO_{ads} and O_{ads} has been found to exhibit the maximum rate of CO_2 production. The initiating role of a reversible phase transition Pt(1 0 0)-(hex) ↔ (1 × 1) was established for the generation of regular waves along certain crystallographic directions on the Pt tip surface: (i) the CO_{ads} wave follows the path in the direction (1 1 1) → (1 1 3) → (1 0 0); (ii) the O_{ads} wave moves through (1 0 0) → (2 1 0) → (1 1 0) faces. The Pt(1 0 0) surface presented by (1 × 1) phase is catalytically active due to its ability to dissociate O_2 molecules. Monte Carlo simulations of the dynamic processes (self-oscillations, waves) on Pt(1 0 0) surface vividly show, that the maximum rate of CO_2 formation is attained in a narrow zone between O_{ads} and CO_{ads} layers, in accordance with our FEM and FIM results. In this reaction zone the highest concentration of free Pt-centres is reached which contributes to dissociative adsorption of O_2 and a rapid reaction with closely arranged CO_{ads} molecules.

3.2. Subsurface oxygen: Pd tip experiments and modeling

In contrast to the Pt(1 0 0) surface, the clean Pd(1 1 0) surface does not change its surface structure during catalytic CO oxidation, and the oscillations in reaction rate are associated with the periodic formation and the consumption of subsurface oxygen $O_{ads} \Leftrightarrow O_{sub}$, which affects the catalytic properties of the metal surface [2–4]. X-ray photoelectron spectroscopy (XPS), temperature programmed reaction (TPR), molecular beam (MB) studies demonstrate the importance of O_{ads} diffusion for the formation of the subsurface oxygen O_{sub}, which is an important intermediate species in the CO + O_2 oscillatory reaction on a Pd tip [21]. O_{ads} is highly active compared to O_{sub} species due to the rapid reaction with CO_{ads}.

3.2.1. Pd tip: FEM

Isothermal, non-linear dynamic processes for the CO + O_2 reaction on Pd tips, as well as the formation of face-specific adsorption islands and the mobility of reaction/diffusion fronts, were studied by FEM [21]. The initiating role of Pd{1 1 0} nanoplanes for the generation of surface waves on the Pd tip was established. Fig. 10A shows the time series of FEM current variations detected when a Pd tip was exposed to a CO + O_2 reaction mixture at 425 K. The oscillations obtained when going from CO_{ads} (low current) to O_{ads} (high current) layers have a period of approximately 5 s. The lines (a–d) in the time sequence, Fig. 10A, mark the corresponding video frames in Fig. 10B (0–5 s). The difference in the work function between the CO_{ads} and O_{ads}

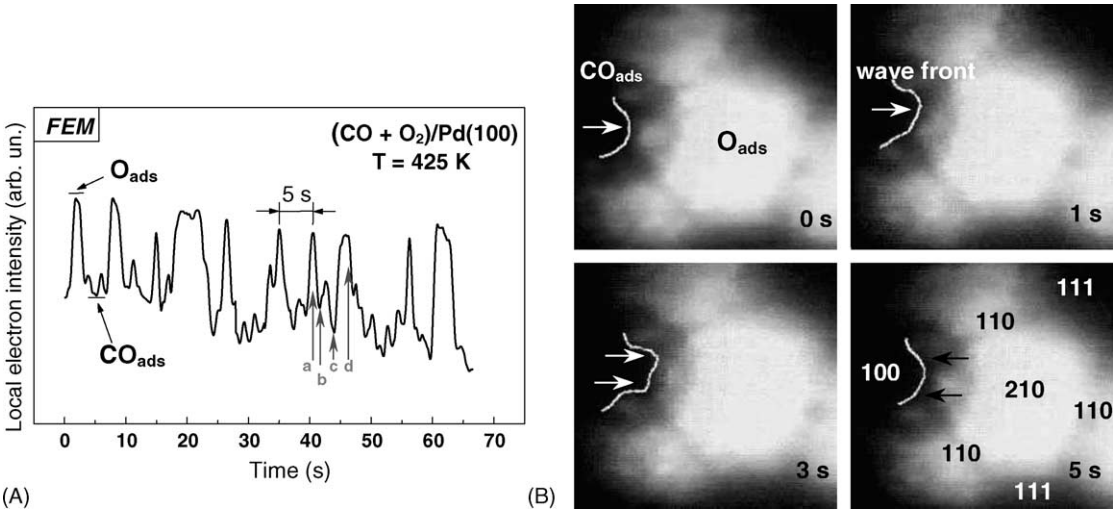

Fig. 10. (A) Variation of the local emission current from the $(1\,0\,0)_{step}$ plane of a Pd tip as a function of time during the oscillatory behaviour of the $CO + O_2$ reaction at $T = 425$ K, $P(O_2) = 2.6 \times 10^{-3}$ mbar, $P(CO) = 1.3 \times 10^{-4}$ mbar. Low current levels reflect CO_{ads}-covered Pd(1 0 0) planes; $F \approx 0.4$ V/Å. (B) Magnified view of a sequence of FEM-images on an (1 1 0)-oriented Pd tip obtained during the $CO + O_2$ oscillating cycle at $T = 425$ K, $P(O_2) = 2.6 \times 10^{-3}$ mbar, $P(CO) = 1.3 \times 10^{-4}$ mbar. At $\tau = 0$–3 s, the formation of a large CO_{ads}-island (dark area on the (1 0 0) plane) and oxygen O_{ads} adsorbs on the (2 1 0) plane (bright area). Reaction front (depicted by thin white line) during regular oscillations starts at the (1 0 0) and moves towards the (2 1 0) plane. After 3 s, the CO_{ads} layer reaches its final island size. After 5.0 s, a reverse reaction front starts from the (2 1 0) towards (1 0 0) plane [21].

covered surfaces of ~0.6 eV leads to these electron current intensity changes. The analysis of Pd tip surfaces with a local resolution of ~20 Å shows the appearance of a sharp boundary between the mobile CO_{ads} and O_{ads} fronts, see Fig. 10B. It was demonstrated that the subsurface oxygen formation also acts as a source in the generation of chemical waves on the Pd tip surface. Two conclusions can be made from these experiments: (i) the maximum initial rate was observed on the {1 1 0} plane, (ii) two spatially separated adlayers are formed on the surface of the tip [21]. Oxygen layers form only on the {1 1 1}, {1 1 0}, {3 2 0} and {2 1 0} planes, whereas CO_{ads} layers form on the {1 0 0} and $\{1\,0\,0\}_{step}$ planes. The O_{ads} and CO_{ads} layers interact via a sequence of reaction steps, including a reversible $O_{ads} \leftrightarrow O_{sub}$ transition, which acts as the feedback mechanism during the oscillations, which is the origin of chemical waves.

3.2.2. Modeling of oscillations and wave patterns

The catalytic oxidation of CO on palladium surfaces exhibits temporal oscillations under a certain range of reaction parameters, T and P_i. The feedback mechanism for these oscillations is associated with the variation of the sticking probability of oxygen (S_O), with the concentration of the subsurface oxygen (Pd(1 1 0): $O_{ads} \leftrightarrow O_{sub}$). The ''oxide'' model [3] assumes that the O_{sub} layer simultaneously blocks oxygen adsorption and helps the growth of CO_{ads} layers, leading to surface reaction poisoning (low rate of CO_2 formation). Nevertheless, a slow reaction of CO_{ads} with O_{sub} removes the subsurface oxygen [21] and O_2 adsorption again becomes possible (high rate of CO_2 formation). Then, the subsurface oxygen layer starts to form again and the cycle is restored. The subsurface oxygen induces significant changes in the adsorption energies of CO_{ads} and O_{ads} [59]. Based on our TPR, XPS, MB and FEM data concerning the CO oxidation on Pd surfaces [21], some elementary steps have been added to the classic LH scheme, namely, Scheme 2.

Here, * and $*_v$ indicate the active sites on the surface and in subsurface layers, respectively. The first step describes the irreversible oxygen adsorption; the second step represents the CO adsorption and desorption processes. The third step corresponds to the reaction between CO_{ads} and oxygen atoms O_{ads}. The formation of the subsurface oxygen proceeds via step 4. The reaction between the nearest neighbour CO_{ads} molecules and the subsurface oxygen is described by step 5. The formation of a complex of CO_{ads} molecules with dissolved oxygen in the form $CO_{ads}O_{sub}$ occurs both via the direct adsorption of CO from the gas phase over the dissolved oxygen (step 6), and via CO diffusion along the surface. The decomposition of the $CO_{ads}O_{sub}$ complex is accompanied by the formation of CO_2 molecules and the appearance of free adsorption sites * and $*_v$ (step 7). We suppose that the heat of CO adsorption on the ''oxidized'' centres $*O_{sub}$ is less than that on the initial centres marked as *, i.e. the probability of $CO_{ads}O_{sub}$ desorption (step 6) is larger than the probability of CO_{ads} desorption (step 2). The adsorbed CO_{ads} species can diffuse

Atomic oxygen route

(1) $O_{2\,gas} + 2* \rightarrow 2O_{ads}$

(2) $CO_{gas} + * \leftrightarrow CO_{ads}$

(3) $CO_{ads} + O_{ads} \rightarrow CO_{2\,gas} + 2*$

Subsurface oxygen route

(4) $O_{ads} + *_v \rightarrow *O_{sub}$

(5) $CO_{ads} + *O_{sub} \rightarrow CO_{2\,gas} + 2* + *_v$

(6) $CO_{gas} + *O_{sub} \leftrightarrow CO_{ads}O_{sub}$

(7) $CO_{ads}O_{sub} \rightarrow CO_{2\,gas} + * + *_v$

Scheme 2.

over the surface according to the following rules: (i) $CO_{ads} + * \leftrightarrow * + CO_{ads}$, (ii) $CO_{ads} + *O_{sub} \leftrightarrow * + CO_{ads}$ O_{sub},(iii) $CO_{ads}O_{sub} + *O_{sub} \leftrightarrow *O_{sub} + CO_{ads}O_{sub}$. According to the applied algorithm of simulation [60–63] that means that CO_{ads} can diffuse over the surface states * and $*O_{sub}$ with equal probability. The sequence of steps 1–5, well known as the Sales–Turner–Maple (STM) mechanism [64], is often used for mathematical modeling of the oscillatory CO oxidation reaction. For a recent review on mathematical models of the STM mechanism, both deterministic and stochastic, we refer to [65]. In our study, in addition to steps 1–5, the possible process of the formation of the $CO_{ads}O_{sub}$ complex has been considered. It was supposed that this complex is formed via CO adsorption (step 6) and via CO_{ads} diffusion over the surface (ii and iii). Step 4 is supposed to be irreversible.

The following mechanism of an oscillatory cycle has been proposed: (i) O_{sub} formation takes place only on the O_{ads} covered palladium surface accompanied by a decrease of the sticking coefficient for oxygen adsorption S_{O_2}; (ii) the formation of a CO_{ads} layer is the result of the slow reaction of $CO_{gas} + *O_{sub}$ with the formation of CO_2 molecules and their desorption, steps 6 and 7; (iii) an elevated concentration of the empty active sites appears due to slow reaction of O_{sub} with CO_{ads} with the formation of CO_2; (iv) the transition to the initial oxygen layer proceeds due to the increase of oxygen sticking coefficient S_{O_2} due to the decrease of O_{sub} concentration.

The dynamic behaviour of the system was simulated with the help of the Monte Carlo method. The details of the procedure were described in [61–63]. The reaction rate of CO oxidation and the surface coverages were calculated after each MC step as a ratio of the amount of CO_2 molecules formed (or the number of lattice cells in the corresponding state) to the overall amount of cells, N^2. It is known that CO adsorption or the dissociative adsorption of oxygen leads to the added/missing row reconstruction of the Pd(1 1 0) plane $(1 \times 1) \rightarrow (1 \times 2)$. As a result, the diffusion of CO_{ads} molecules along the rows of metals atoms occurs more rapidly than across the rows. We found that the propagation of a wave on the Pd(1 1 0)-(1×2) surface becomes noticeably anisotropic. Fig. 11 shows images of the adsorbed layer in the case of the spiral wave during the reaction of CO oxidation on Pd(1 1 0). Fig. 11a shows the simulated form of a spiral wave at the moment when the anisotropy of diffusion starts to work. Fig. 11b and c show how spiral waves extend after passing through the first and second turns of the spiral. Such an asymmetric behaviour of the spiral waves agrees well with experimental data presented in Fig. 11d and which were obtained using the PEEM [66].

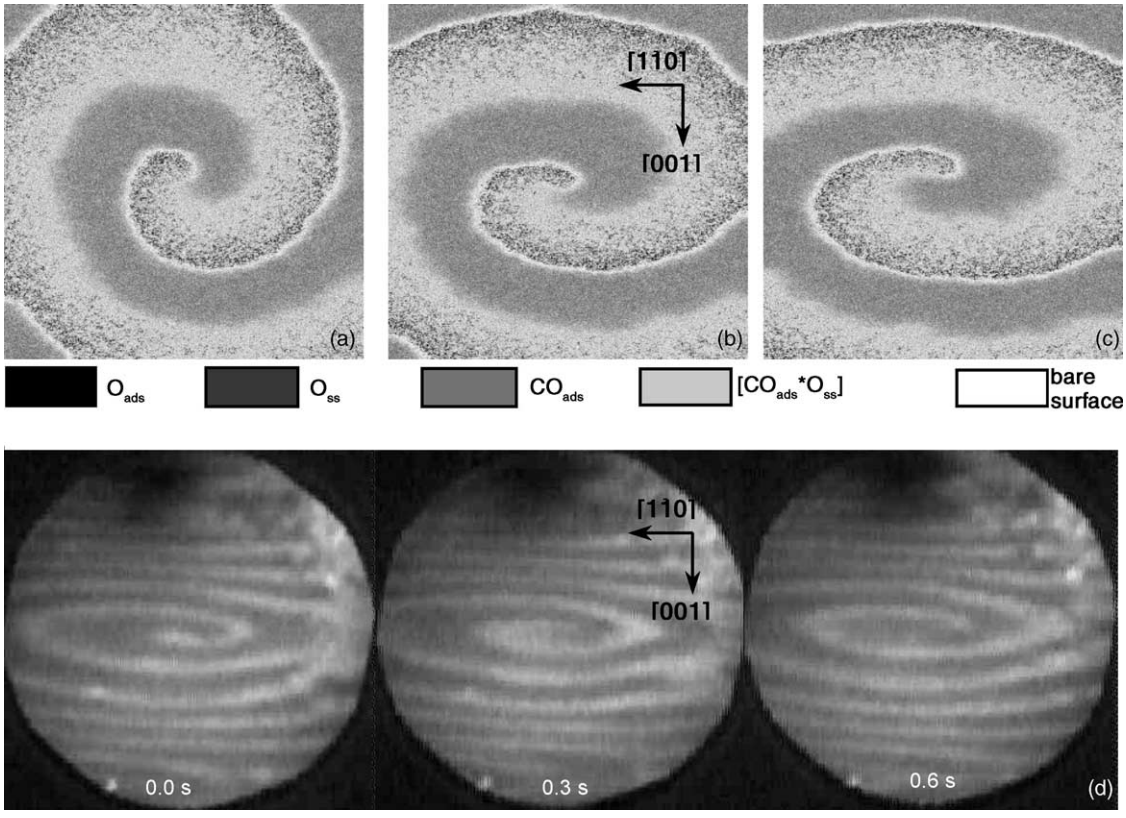

Fig. 11. Simulation results of the variation of the form of a spiral wave during CO oxidation on a Pd(1 1 0) surface after the transition from the regime with isotropic diffusion (M_x/M_y = 50/50) to anisotropic (M_x/M_y = 80/20), N = 1536: (a) isotropic diffusion; (b) after the first turn of the spiral; and (c) after the second turn [31]. (d) Experimentally observed PEEM images of the surface in the case of the existence of a spiral wave during CO oxidation on a Pd(1 1 0) single crystal plane. Dark regions indicate CO_{ads}; light regions indicate O_{ads} [66].

3.2.3. Summary

In the present work, the mechanism of the generation of surface waves during the oscillating CO + O_2 reaction has been studied on a Pd tip (∼2000 Å in radius) by FEM. On the oxidized surface (containing large amount of O_{sub}) oscillations on the Pd(1 0 0)$_{step}$ nanoplanes can be obtained with fast periods. Analysis of the tip surface shows the availability of a sharp boundary between mobile CO_{ads} and O_{ads} fronts. A maximum initial rate has been observed on Pd(1 1 0) nanoplanes and two spatially separated adlayers are formed on the tip surface. The oxygen layer only forms on the {1 1 0}, {3 2 0} and {2 1 0} planes, whereas CO_{ads} layers or empty sites form on the {1 0 0} and {1 0 0}$_{step}$ planes. Chemical waves are associated with the diffusion of O_{ads} and CO_{ads} species and with the reversible transition of the adsorbed oxygen into the subsurface layer $O_{ads} \leftrightarrow O_{sub}$. The feedback mechanism is based on the formation and the removal of the subsurface oxygen. Monte Carlo simulations, which were based on this reaction mechanism for the Pd(1 1 0) surface demonstrate the appearance on the catalyst surface of turbulent patterns, spiral and elliptic waves [31].

4. Chemical waves in catalytic H_2 oxidation

4.1. Phase transitions of Pt(1 0 0)-hex ↔ 1 × 1: Pt tip experiments

For H_2 oxidation, regions of bistability have already been predicted by theory [45]. Chemical wave patterns have been found on Rh(5 3 3) [67], Rh(1 1 1) [68], Rh(1 1 0)/Pt [69] surfaces by PEEM, on Ir and Rh tip surfaces by FEM [70,71] and on Pt(1 1 1) surface by STM [72]. In the FIM images different regimes of catalytic activity, and kinetic oscillations have been observed, at certain control parameters (T, P) [73]. In our work [17,39,73] the reacting gases at the catalyst surface have been used to image the surface "in situ". Fig. 12A displays the oscillatory behaviour with a period of ∼30 s [44]. In Fig. 12B-a–l, the sequence of "in situ" FIM images at 300 K demonstrates how chemical waves can develop during the oscillatory catalytic oxidation of hydrogen [17]. The different levels of brightness indicate the different adsorption layers on the surface. The areas with medium brightness represent O_{ads} layers imaged by O_2^+ ions; very bright regions indicate areas with a high production rate of H_2O; dim areas are covered by H_{ads}. The oscillation cycles start with an O_{ads} layer (a) that shows the formation of a highly reactive zone yielding H_2O (H_2O^+/H_3O^+) product molecules in the central (0 0 1) plane. This zone spreads rapidly over the whole surface (b–e), including a Pt(1 0 0)-(1 × 1) surface at this stage. Due to the high reactivity of the Pt(1 0 0)-(1 × 1) surface, the coverages of both reacting species become rather low. As a consequence, the (1 × 1)-surface is no longer stable but transforms into the hexagonal phase (f and g). Because the sticking coefficient for O_2 is much lower on the Pt(1 0 0)-hex surface, build-up of a H_{ads}-layer takes place resulting in the lifting of the hexagonal reconstruction back to the (1 × 1) phase (h–l). The transition of the Pt(1 0 0)-hex into the Pt(1 0 0)-(1 × 1) surface is combined with a change in the density of the top Pt layer and during this process about 20% of its atoms are ejected [74]. This process is visible "in situ" and manifests itself by the appearance of fluctuating small Pt clusters (brighter spots) that can be discerned in the image (g). The H_{ads} regions still appear dim in the FIM images and shrink in diameter (k and l), until the surface is again completely covered with oxygen as at (a). During this oscillatory behaviour, the imaging process has been combined with mass spectrometry and field ion appearance energy spectroscopy measurements [39]. The reconstruction

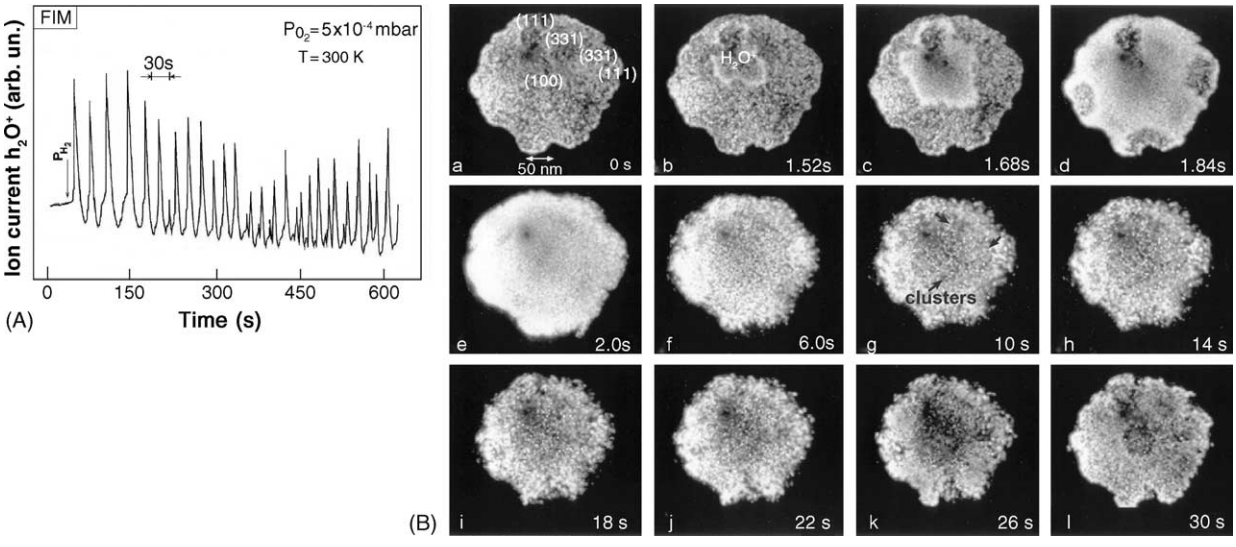

Fig. 12. (A) Oscillatory behaviour during the $H_2 + O_2$ reaction on an [0 0 1]-oriented Pt tip with 1800 Å radius at 300 K and $P(O_2) = 5 \times 10^{-4}$ mbar, $P(H_2) = 6 \times 10^{-4}$ mbar. (B) A sequence of FIM images during the H_2 oxidation at 300 K; $F \approx 1.5$ V/Å. Imaging gases are O_2 from the reactants and H_2O formed during the reaction. The time internals after the initial image (O_s) is given at the lower right corners of the images [17].

in the (1 0 0) plane represents the sequence:

$$O_{ads}(1 \times 1)Pt \xrightarrow{H2} H_2O_{gas}$$
$$+ \text{hex}\,Pt \xrightarrow{H2} H_{ads}(1 \times 1)Pt \xrightarrow{O2} H_2O_{gas} + O_{ads}(1 \times 1)Pt$$

Thus, we can conclude that during oscillations the catalytic reaction is creating and destroying its own active centres on the surface of the catalyst. These results demonstrate that the critical size of surface nanoplanes for which rate oscillations and other collective phenomena can be observed, is very small. Probably even less than ~200 Å size is sufficient for the generation of chemical waves. Recently, using Monte Carlo simulations [75,76], it was predicted that for the disappearance of non-linear phenomena (hysteresis, bistability, oscillations) the nano-planes must contain less than ~100–200 surface sites.

4.2. Modificating effect of defects on Pt(1 0 0) with respect to H_2 and O_2 adsorption

At 300 K, no hydrogen could be adsorbed on the reconstructed Pt(1 0 0)-(hex) surface [77]. At $T < 300$ K, H_2 adsorption leads to characteristic changes in the surface structure: the (hex) → (1 × 1) reconstruction is observed. According to our HREELS study reported in ref. [77], the low temperature desorption peaks (190, 240 K) which are related to the two low frequency bands at 555 and 820 cm^{-1}, originate due to the population of the residual (hex) patches and defects created in the course of the hex → (1 × 1) phase transition. It has been established that the obtained H/(1 × 1)-like structure, however, does not represent a perfect (1 × 1) phase, since it contains a certain concentration of structural defects and residual (hex) patches remain as well on the surface [78]. The concentration of the defect sites and (hex) patches for saturated H_{ads} layer at 90 K (~1.2 ML) corresponds to ca. 20% of the total hydrogen layer [77].

Fig. 13b shows HREEL spectra of an atomic oxygen layer which formed i) after a 3 L NO exposure on the reconstructed Pt(1 0 0)-(1 × 1) surface at 300 K with a further temperature increase up to 500 K for NO_{ads} desorption and ii) after the titration reaction $O_2 + H_{ads}$/Pt(1 0 0)-(hex) at 220 K [58]. The band at 540 cm^{-1} represents ν(PtO) stretching of adsorbed atomic oxygen as a result of NO dissociation on defect sites. For example, on a flat Pt(1 1 1) surface a single ν(PtO) band is observed at 460 cm^{-1} after O_2 adsorption at 250 K. Fig. 13a and Fig. 13b show that the interaction of an atomic hydrogen layer H/Pt(1 0 0)-(hex) with preadsorbed oxygen molecules (220 K, 30 L) is accompanied by the formation of an oxygen layer (O_{ads}) with Pt–O bond vibration frequencies of 460, 720 and 920 cm^{-1}. According to TDS data, the main desorption O_2 peak is observed around 710 K. Comparable TDS results were obtained for the Pt(1 0 0)-(hex) surface after oxygen exposure at high temperature (575 K, 3×10^5 L): two desorption peaks at 660 and 710 K were observed. In agreement with the experimental data for oxygen adsorption

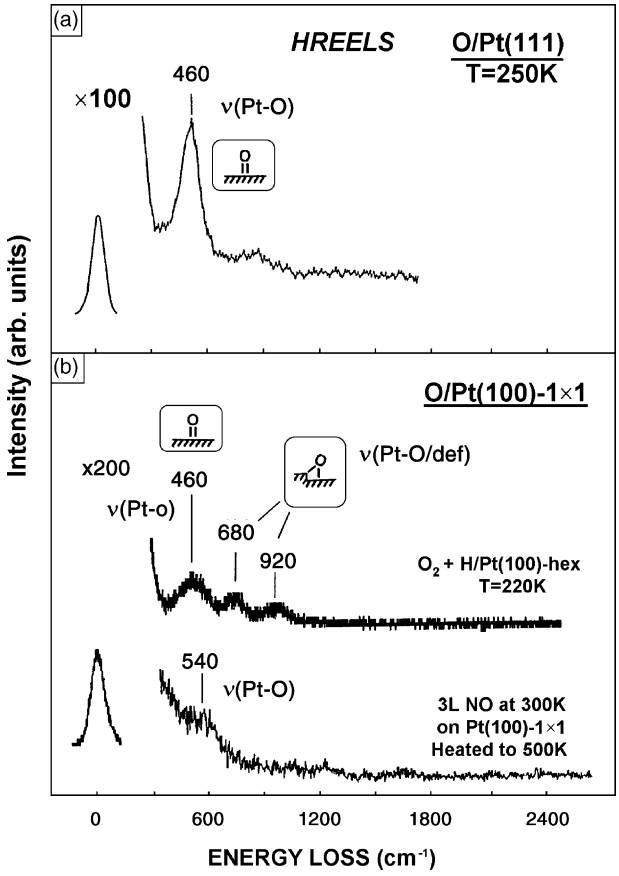

Fig. 13. (a) HREEL spectrum obtained after a 9 L O_2 exposure on a Pt(1 1 1) surface at 105 K and subsequent heating in vacuum up to 250 K. (b) HREEL spectra (i) for atomic oxygen forming as a result of H_{ads} titration by oxygen (30 L) on a Pt(1 0 0)-(hex) surface at 220 K; (ii) for the atomic oxygen produced by NO dissociation on the Pt(1 0 0)-(1 × 1) surface at 300 K [58].

on the Pt(3 2 1) single crystal surface [79] the bands at 720 and 920 cm^{-1} can be attributed to oxygen atoms adsorbed on structural defects (presumably steps or kinks) induced by the O + H reaction. These bands can serve as a good spectral indicator of the strong structural transformation of the Pt (1 0 0)-(hex) surface.

4.2.1. Summary

For the $H_2 + O_2$/Pt system, the observed character of oscillating behaviour differs remarkably from that in CO oxidation: (i) product water molecules (H_2O^+/H_3O^+ ions) directly show the catalytically active sites; (ii) H_{ads}- and O_{ads}-fronts move in reverse directions. The hydrogen-modified Pt(1 0 0)-(hex) surface shows an increase in both the population of atomic oxygen states at the $H_2 + O_2$ reaction and the reactivity of oxygen atoms towards H_2 for the formation of H_2O. The nature of the defects has not been directly investigated, but chemically the defect sites behave like kinks and steps on a Pt(1 0 0) surface. These results may lead to a better understanding of the mechanism of rate oscillations in the $H_2 + O_2$ reaction on the nano-Pt(1 0 0) surfaces. By means of field ion appearance energy spectro-

scopy only a minor influence of the electric field on the kinetics of H_2 oxidation on Pt tip surfaces could be achieved [46].

5. Chemical waves in catalytic NO + H_2 reaction

5.1. FEM: Rh tip experiments

Automotive three-way catalysts based on Pt–Rh are preferred because of the higher degree of NO_x reduction under fuel rich conditions [7,80]. It has been shown that the mechanism of the non-linear behaviour in the NO + H_2 reaction on Pt, Rh and Ir surfaces involves the creation of adjacent vacant sites needed for NO dissociation. The products N_2, N_2O, NH_3, H_2O, leaving the surface facilitate an autocatalytic increase of the concentration of such vacant sites and, hence, lead to an autocatalytic increase of the reaction rate [6]. The availability of vacant sites near the NO_{ads} and N_{ads} may play a central role in the selectivity towards N_2O and N_2. For NH_3 formation surface vacant sites are needed for H_2 dissociation and the subsequent reaction of H_{ads} with N_{ads}.

The first observations with FEM of the spatiotemporal behaviour during the NO + H_2 reaction have been made for Rh [8,27,29,81]. It also resulted in the discovery of macroscopic rate oscillations on extended Rh single crystal planes [80,82]. Rh is the most efficient catalyst for the selective reduction of NO_x to nitrogen. The basic mechanism of the ''vacancy'' model [27] involves the following steps: (i) the initial surface coverage of NO is sufficiently high and inhibits NO dissociation and the reaction; (ii) due to NO desorption or reaction between O_{ads} and H_{ads} some free sites or vacancies are created; (iii) the neighbouring NO molecules can now dissociate and leave their O_{ads} atoms on the vacancies; (iv) the concentrations of N_{ads} and O_{ads} atoms increase and at a certain stage inhibit NO dissociation. As a result, the NO_{ads} coverage increases and the system returns to its initial state, completing the oscillating cycle.

To explain the structure of Rh tip, Fig. 14B shows the position of some crystal planes present on Rh tip. After the introduction of the reactant mixture containing 2×10^{-7} mbar NO and 1.3×10^{-6} mbar H_2, the temperature was slowly decreased from 530 to 460 K until oscillations were observed. The appearance of a characteristic ''fence-like'' image (Fig. 14B-a) was observed at $\tau = 0$. NO molecules nearly completely cover the Rh surface. The FEM image presented in Fig. 14B-b at $\tau = 1$ s shows the appearance of a bright spot in the emission pattern. A surface ''explosion'' begins on the (3 2 1) surface due to the autocatalytic character of the reaction: NO_{ads} can dump its O_{ads} atom on the vacancies created, and H_2 molecules can also adsorb and dissociate, followed by very fast reactions between N_{ads} and or NO_{ads} and between O_{ads} and H_{ads} to form N_{2gas} and H_2O_{gas}, respectively [steps (5–7) of the reaction scheme]. Fig. 14B-c at $\tau = 2.9$ s show that the reaction spreads across the surface into the direction of (3 1 0). As can be seen from Fig. 14B-d–f the reaction fronts move symmetrically from two sides across the surface until at $\tau = 14$ s, the reaction occurs on the entire surface. The observed sharp moving front mainly displays the hydrogenation of the atomic nitrogen layer, followed by the decomposition and or the recombination of intermediate $NH_{x(ads)}$ species, which then can restore the surface coverage

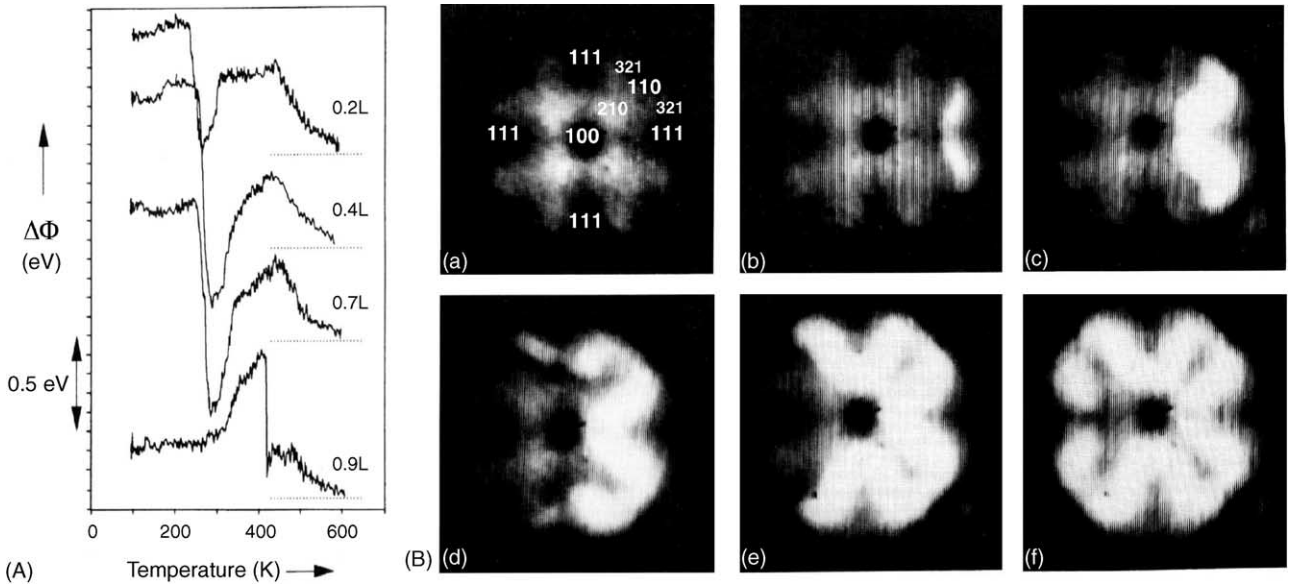

Fig. 14. (A) Dependence of the change in work function of the (3 3 1) surface on a Rh tip during the NO_{ads} + H_2 reaction and temperature. The dotted lines indicate the work function of a clean (3 3 1) Rh surface (from ref. [35]). (B) Some of the FEM images recorded during oscillatory behaviour of the NO + H_2 reaction on a Rh tip: (a) the characteristic image of the initial state of the Rh tip with the indication of the principal faces, $\tau = 0$ s; (b) $\tau = 1$ s; (c) $\tau = 2.9$ s; (d–f) the reaction fronts move symmetrically across the surface from two sides; (f) $\tau = 14$ s [81].

of N_{ads} via the $NO + H_2$ reaction [29]. It is likely that $NH_{x(ads)}$ species decreases the work function (WF) due to the strong negative WF change caused by NH_3 adsorption [81]. Therefore, the WF drop shown in Fig. 14A can be attributed to the formation of intermediate $NH_{x(ads)}$, which then decomposes forming a nitrogen layer with further N_2 desorption at elevated *T*. After the last step is completed the FEM image becomes dark again due to a restoration of the initial adlayer due to NO adsorption, see Fig. 14B-a. It was found that the influence of the wave front is only confined to a very small region, the wave moves like a ''one-dimensional'' snake over the surface, its length is increasing but its width is constant. Note that under these conditions the (1 0 0) planes do not contribute to the oscillations. The oscillations are very stable for many hours since in this case the reaction mixture does not contain any component that can inhibit the oscillations completely. The applied field does not influence the oscillations noticeably. It was shown that a variation of the field strength during oscillations, or switching on and off the applied field did not influence the oscillations to a measurable extent. Many investigations were devoted to the oscillatory behaviour of the $NO + H_2$ reaction under different NO/H_2-ratios. The study of the $NO + H_2$ reaction on Rh tip demonstrated that in $NO/H_2 = 1/13$ ratio the temperature at which oscillations are observed is lower than at $NO/H_2 = 1/6.5$ [81]. It was also shown that the period of the oscillations decreases when more H_2 is present.

As was shown in ref. [83] the main reaction mechanism can include the following steps:

1. $NO_{gas} + * \rightarrow NO_{ads}$
2. $NO_{ads} + 2* \rightarrow N_{ads} + O_{ads}$
3. $H_{2gas} + 2* \rightarrow 2H_{ads}$
4. $N_{ads} + 3H_{ads} \rightarrow NH_{3gas} + 4*$
5. $2H_{ads} + O_{ads} \rightarrow H_2O_{gas} + 3*$
6. $2N_{ads} \rightarrow N_{2gas} + 2*$
7. $NO_{ads} + N_{ads} \rightarrow N_{2gas} + O_{ads} + *$
8. $NO_{ads} + N_{ads} \rightarrow N_2O_{gas} + 2*$

The symbol * stands for a vacancy (empty site). The first step in the formation of N_2, N_2O, and NH_3 is NO dissociation. The selectivity for the formation of N_2, N_2O, and NH_3 depends on the relative concentrations of N_{ads}, H_{ads} and NO_{ads} on the surface [83]. N_2O is formed under conditions with high concentrations of molecularly adsorbed NO (low temperatures), N_2 formation requires a relatively high concentration of N_{ads} on the surface and NH_3 production is high when the concentration of N_{ads} is relatively low. An excess of hydrogen favors NH_3 formation.

It was found earlier [84] that on Rh(1 0 0) the rate of NO conversion is low at temperatures below 600 K due to the high concentration of strongly bound N_{ads} atoms, blocking the surface for reaction. The rate-limiting step is the dissociation of NO in step (2) that requires vacant sites in order to proceed. Since the subsequent steps (4–6) are fast, an autocatalytic increase in the concentration of vacant sites is responsible for the occurrence of a ''surface explosion'' on the (3 2 1) plane (Fig. 14b), which initiates the formation of a reaction front over spatially adjacent regions (Fig. 14c–f). Oxygen atoms O_{ads} are also present on Rh(1 0 0) during $NO + H_2$ reaction. However, the O_{ads} does not block the surface active sites. Probably, the oxygen atoms are situated beneath the surface while the concentration of O_{ads} is low. Since the Rh(1 1 0) [85] and Rh(5 3 3) [86] single crystal surfaces are also known to show non-linear behaviour in the $NO + H_2$ reaction, it is relevant to compare the results obtained for these single crystal planes with the results reported for the Rh(1 0 0) surface. It was demonstrated that the origin of the difference between Rh(1 0 0) and Rh(1 1 0), Rh (5 3 3) is connected with the difference of the Rh–N bond strength for the various single crystal planes [86]. It was found that the oscillatory behaviour on Rh(5 3 3) originated due to relatively weakly bound nitrogen, whereas no oscillations were found on Rh(1 0 0). Strongly bound nitrogen species inhibit the oscillatory behaviour on this surface. Destabilization of the N_{ads} layer by O_{ads} and suppression of hydrogen adsorption by N_{ads} were considered to be the key elements in the excitation mechanism of the chemical waves observed around 530 K on Rh(1 1 0) [86,87]. Simulations of the oscillations in the $NO + H_2$ reaction on Rh(5 3 3) have demonstrated that lateral interactions between the species adsorbed on the surface may play a key role in the mechanism of oscillations [88].

The traveling waves demonstrate the large role of hydrogen H_{ads} diffusion for the communication between the different surfaces during the oscillatory behaviour. It was shown that the nature of the wave fronts is not a diffusion of reaction products or intermediates, but the removal of the adlayer by the reaction of NO and its dissociation fragments with hydrogen [27]. The anisotropy of the traveling waves along the {1 1 3} planes could be explained by the anisotropic diffusion of hydrogen, which is faster parallel to the step edges.

5.2. FEM:Pt tip experiments

Isothermal oscillations on a Pt tip in the $NO + H_2$ reaction have been observed by FEM at pressures around 1×10^{-5} mbar NO and 1×10^{-5} mbar H_2 at 416 K [23]. Fig. 15a and b shows the FEM images during these transient oscillations, where all the stepped areas around three (1 0 0) nanoplanes present on the (1 1 1)-oriented Pt tip are oscillating in phase with each other. The oscillations began as an increase in the emission current (white rings, b) over the entire stepped surfaces around the (1 0 0) plane with a period of ~70 s. In some cases, it was possible to see that the ring did not homogeneously increase in intensity, but that the area around (5 1 0) was first to increase. This behaviour was only transient, because no more than 20 oscillations could be

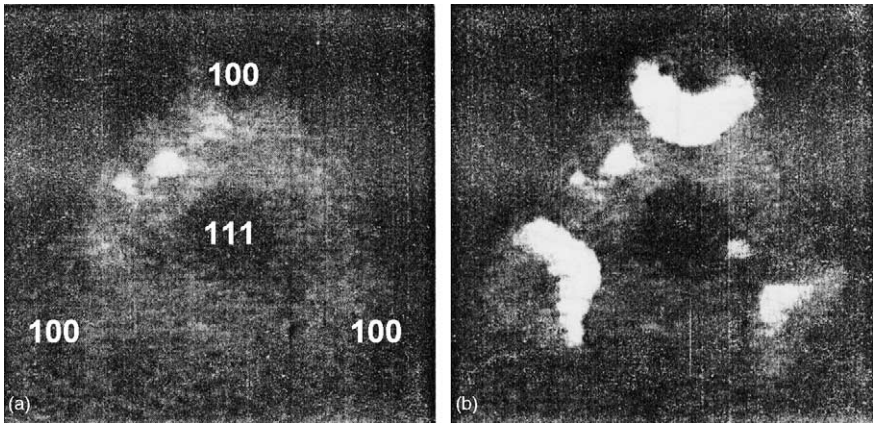

Fig. 15. FEM images recorded during the NO + H_2 reaction on a Pt tip surface at 416 K, $P(NO) = 1 \times 10^{-5}$ mbar and $P(H_2) = 1 \times 10^{-5}$ mbar. Images taken at (a) 0 s and (b) 5 s [23].

detected. As can be seen from Fig. 15b, the (1 1 1) nanoplanes were not involved into the oscillatory process. The brightening of the (1 0 0) regions originates due to the formation of reaction intermediates or reaction products. Both NH_{3ads} and $NH_{x(ads)}$ ($x = 1$ or 2) species cause a strong decrease in the work function.

On platinum surfaces the adsorbed state of NO may be of a molecular or dissociative nature, depending on the surface structure [80], which thereby determines the details of the NO + H_2 reaction mechanism and the key products—N_2 or NH_3. Our analysis of the corresponding ν(NO) band positions [89] showed that NO adsorption on the Pt(1 1 1) single crystal plane proceeds only molecularly in two- or three-fold bridge and on-top states. HREELS and TDS results conformed that NO desorbs completely from Pt(1 1 1) without dissociation. However, N_2 and NH_3 formation were found upon heating the NO-covered Pt(1 1 1) surface in a hydrogen atmosphere. It was demonstrated that NO molecules adsorbed in the bridge form take part in these reactions. HNO_{ads} and N_{ads} surface species have been observed as reaction intermediates [89]. This is an example of the so-called ''molecular mechanism'', which proposed an additional pathway for the hydrogen-associated NO dissociation illustrated by the equations of the reaction. HREELS studies of the NO + H_2 reaction on Pt(1 0 0) demonstrated that the formation of NH_3 proceeds via an $NH_{x(ads)}$ intermediate [90,91]. The N_2 and H_2O products are formed, when the concentration of $NH_{x(ads)}$ is low. The rate determining step on the Pt(1 0 0) surface is an activated step of NO dissociation occurring at $T \geq 400$ K. N_{ads} atomic layer on the Pt(1 0 0) surface is highly active and readily reacts with hydrogen at 300 K producing NH_{3ads}. The comparison of intermediates formed on different surfaces – HNO_{ads}/Pt(1 1 1) [89], NH_{ads}/Pt(1 0 0)-hex [90], NH_{2ads}/Pt(1 0 0)-1 × 1 [91] – allows one to establish the features of molecular and dissociative mechanisms in catalysis. The molecular and dissociative mechanism of the NO + H_2 reaction can be written as follows:

Molecular mechanism, Pt(1 1 1) (no oscillations)	Dissociative mechanism, Pt(1 0 0) (oscillations)
1. $NO_{gas} \leftrightarrow NO_{ads}$	1. $NO_{gas} \leftrightarrow NO_{ads}$
2. $H_{2gas} \leftrightarrow 2\ H_{ads}$	2. $H_{2gas} \leftrightarrow 2\ H_{ads}$
3. $H_{ads} + NO_{ads} \rightarrow HNO_{ads}$	3. $NO_{ads} \rightarrow N_{ads} + O_{ads}$
4. $HNO_{ads} + H_{ads} \rightarrow N_{ads} + H_2O_{gas}$	4. $O_{ads} + 2\ H_{ads} \rightarrow H_2O_{gas}$
5. $N_{ads} + 3\ H_{ads} \rightarrow NH_{3ads}$	5. $N_{ads} + 3\ H_{ads} \leftrightarrow [NH_{ads}] \rightarrow NH_{3gas}$
6. $N_{ads} + N_{ads} \rightarrow N_{2gas}$	6. $N_{ads} + N_{ads} \rightarrow N_{2gas}$

Kinetic oscillations during the NO + H_2 reaction on the extended Pt(1 0 0) surface were observed for reactant partial pressures in the range 10^{-6}–10^{-5} mbar and temperature interval from 430 to 500 K [92–97]. Multiplicities of steady states associated with hysteresis phenomena [92,93], and spatial pattern formation [98] have also been observed for this system. The mechanism of oscillations was described in terms of the vacancy model [97]. In the low reactivity state the surface is blocked by NO_{ads}. Vacant sites are needed for NO dissociation and reaction. The important step in this mechanism involves the autocatalytic creation of vacant sites (steps 4–6, dissociative mechanism) required for NO dissociation and, hence, for reaction. Our recent simulations showed that the phase transition Pt(1 0 0)-hex ↔ 1 × 1 is not essential for producing oscillatory behaviour [99,100]. The strongly non-linear dependence of NO_{ads} dissociation on the number of vacant Pt sites is the most important factor.

5.3. FEM: Ir tip experiments

Isothermal oscillations during the NO + H_2 reaction were observed on an [1 1 1]-oriented Ir tip in excess of H_2 at H_2:NO ratios greater than 20, and for P(NO) above 2.3×10^{-6} mbar. All three (1 0 0) nanoplanes that were present on the Ir tip surface were oscillating in phase with each other [23,25]. During oscillatory behaviour, regular variations of the emission current have been observed as a result of moving waves that spread across the (5 1 0) and (1 0 0) surfaces of the tip. The concentric waves start only at the (5 1 0) stepped nanoplanes and travel to the (1 0 0) surfaces. Other planes, namely (1 1 0), (2 1 0) and (1 1 1)

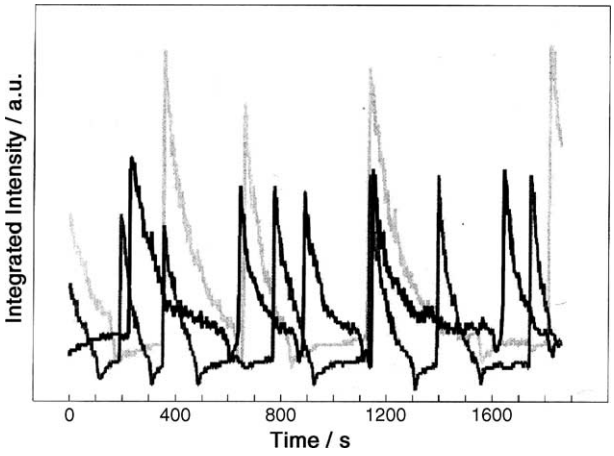

Fig. 16. The integrated intensity of the three different (1 0 0) surfaces present on an [1 1 1]-oriented Ir tip at 354 K, $P(NO) = 2 \times 10^{-6}$ mbar and $P(H_2) = 4.7 \times 10^{-5}$ mbar [25].

did not take part in the moving waves. Fig. 16 shows the variation of the emission intensity from three (1 0 0) surfaces as derived from the video intensity of the digital FEM [34,35]. It can be seen that the three planes operate independently of one another. A similar independent dynamic behaviour due to the presence of fluctuations in the bistable range has been observed during the $CO + O_2$ reaction on the nanoplanes of a Pt tip [101–103].

5.4. Summary

The $NO + H_2$ reaction on Pt, Rh and Ir tip surfaces show a variety of different forms of non-linear behaviour. The mechanism of the local oscillatory behaviour on Pt(1 0 0) nanoplanes is different from that on Rh surfaces: on Pt(1 0 0) the dissociation of NO is rate limiting, whereas on Rh the ability to accumulate N_{ads} in a reversible manner plays a central role. The surface structure of the Rh tip determines the degree of synchronization of local surface oscillators. The oscillations on the Rh(5 3 3) nanoplane initiate the oscillations on the entire Rh tip. The velocity of the reaction fronts on a Rh tip surface is strongly anisotropic with the maximum propagation in the direction parallel to the step $(1\,0\,0)_{st}$ nanoplanes and a minimum velocity is observed in the direction perpendicular to the steps. On a Ir tip a surface wave is initiated first at the (5 1 0) nanoplane and spreads to the surrounding planes. It was shown that the stepped Ir(5 1 0) and Rh(5 3 3) surfaces act as a source for the propagation of wave fronts. A stepped surface is more open, and possibly, more reactive than a flat surface. Such steps can induce high-reactive centres to which surface species may migrate from other less

Table 2
Oscillatory reactions on metal tip surfaces of the Pt-group metals

Reaction	Metal	Method	Trigger centers	Temperature (K)	Conditions	References
$H_2 + O_2$	Pt	FIM	{1 0 0}	300	$P(O_2) = 5 \times 10^{-4}$ mbar $P(H_2) = 6 \times 10^{-4}$ mbar	[17]
$CO + O_2$	Pt	FEM	{1 0 0}	365	$P(O_2) = 5 \times 10^{-4}$ mbar $P(CO) = 8 \times 10^{-6}$ mbar	[18]
	Pt	FIM	{1 0 0}	365	$P(O_2) = 5 \times 10^{-4}$ mbar $P(CO) = 5 \times 10^{-6}$ mbar	[19,20]
	Pd	FEM	$\{1\,0\,0\}_{st}$	425	$P(O_2) = 2.6 \times 10^{-3}$ mbar $P(CO) = 1.3 \times 10^{-4}$ mbar	[21]
$NO_2 + H_2$	Pt	FIM	{2 1 0}	515	$P(NO_2) = 2 \times 10^{-5}$ mbar $P(H_2) = 2 \times 10^{-5}$ mbar	[22]
$NO + H_2$	Pt	FEM	$\{1\,0\,0\}_{st}$	416	$P(NO) = 1 \times 10^{-5}$ mbar $P(H_2) = 1 \times 10^{-5}$ mbar	[23]
	Pt	FIM	{2 1 0}	525	$P(NO) = 2.5 \times 10^{-5}$ mbar $P(H_2) = 3.9 \times 10^{-5}$ mbar	[24]
	Ir	FEM	{5 1 0}	341	$P(NO) = 1.3 \times 10^{-6}$ mbar $P(H_2) = 4.6 \times 10^{-5}$ mbar	[25]
	Ir	FIM	{1 0 0}	349	$P(NO) = 2.4 \times 10^{-6}$ mbar $P(H_2) = 6.2 \times 10^{-5}$ mbar	[26]
	Rh	FEM	{3 2 1}	430	$P(NO) = 1.1 \times 10^{-7}$ mbar $P(H_2) = 1.4 \times 10^{-6}$ mbar	[8,27,28]
	"twin" Rh tip	FEM	$(1\,0\,0)_{def}$	430	$P(NO) = 1.1 \times 10^{-7}$ mbar $P(H_2) = 1.3 \times 10^{-6}$ mbar	[29]
$NO + NH_3$	Rh	FEM	{5 1 1}	594	$P(NH_3) = 4 \times 10^{-7}$ mbar $P(NO) = 1.7 \times 10^{-7}$ mbar	[30]

$(1\,0\,0)_{st}$: stepped surface around (1 0 0) nanoplane; "twin" FEM, $(1\,0\,0)_{def}$: the Rh tip consists of [1 1 1]-oriented twins separated by a (1 0 0) nanoplane. This central (1 0 0) plane is devided into two unequal parts with defects, the grain boundary.

reactive regions. This in turn would induce reaction in these less-reactive regions, because they have become less populated by surface species, leaving active sites, for example, for the dissociation of other species.

6. The surface specificity of the oscillating reactions

The nonlinear behaviour of model reactions ($CO + O_2$, $CO + NO$, NO_x reduction, etc.) on metal tip surfaces of the Pt-group metals was intensively investigated during the last decade, as illustrated in Table 2.

In all of these FEM and FIM studies involving oscillatory behaviour the interactions between adjacent crystal planes of the tip are important for describing the observed phenomena [17–30]. Observation on emitter tips demonstrate that the certain nanoplanes (“trigger centers” [4]) are the most reactive regions and can act as nucleating centers for triggering of the reaction fronts on adjacent planes. In the $H_2 + O_2$ and $CO + O_2$ reactions on a Pt tip studied by FEM/FIM, the Pt(1 0 0) surface was shown to act as a source for propagating wave fronts [17–20]. A study of a Pd tip has shown that the $Pd(1\ 0\ 0)_{st}$ surface was responsible for the generation of a local regular wave in the CO oxidation [21]. The reduction of NO_2 by hydrogen on a Pt tip studied by FIM, demonstrated the explosive ignition on the (2 1 0) planes followed by a reaction front along the channels of the (3 1 1) planes. The global reaction rate revealed self-sustained oscillatory behaviour during this process [22]. In the case of the $NO + H_2$ reaction on a Pt tip in FIM studies, the (2 1 0) plane triggered a short-lived pulse that spread towards the [1 0 0] direction, whereas in FEM studies, only temporary oscillations were seen on the stepped surfaces near the (1 0 0) plane [23,24]. For the $NO + H_2$ reaction, oscillatory behaviour has been observed in FEM/FIM studies on a Ir tip [25,26]. In this case, a chemical wave initiated at the (5 1 0) surface, moved firstly toward the nearby (1 0 0) plane, and then spread to the surrounding stepped planes. For the same reaction on a Rh tip, the Rh(3 2 1) surface triggered an increase in emission that moved around the tip engulfing many, but not all of the present planes [8,27]. Surface peculiarities like steps, ledges and other lattice defects may dramatically influence the catalytic properties of metal surfaces [104,105] and to influence the initiation of the surface waves. During the $NO + H_2$ reaction on a twinned Rh tip, the two tips, separated by a $(1\ 0\ 0)_{def}$ grain boundary, could act synchronously, trigger one another or act independently [29]. The $NO+NH_3$ reaction on a Rh tip also showed interesting oscillatory behaviour: four apparently separate (5 1 1)–(7 1 1) areas of the tip oscillating in phase [30].

7. Conclusions

The present results show that the field electron and field ion microscope can serve as an in situ catalytic flow reactor in the 10^{-7}–10^{-3} mbar total pressure regime. A very fine metal tip, ~1000 Å in radius, exposes particular surface nanoplanes with different structures. The experimental results prove that self-sustained oscillations in the catalytic $H_2 + O_2$, $CO + O_2$ and $NO + H_2$ reactions are observed on the nanoscale on certain surface areas of Pd, Rh, Ir and Pt tips as small as a few hundred surface sites while surroundings with different crystallographic nanoplanes stay in a stationary state. With slightly different external control parameters, mixed-mode oscillations caused by sequential reaction steps occur, characterizing a collective ensemble of crystal nanoplanes. The principal result of our studies is that the phenomena related to oscillatory dynamics of catalytic reactions could be observed not only at macroscopic planes since: (i) planes of ~200 Å in diameter show the same non-linear kinetics; (ii) regular waves appear under the reaction rate oscillations; (iii) the propagation of reaction-diffusion waves includes the participation of the different crystal nanoplanes and indicates an effective coupling of adjacent planes.

The obtained results reveal the detailed mechanism of self-organization in chemical reactions on catalytically active surfaces of hundred Angstroms size. A close connection was established between the experiment and the theory. New experimental data are obtained, concerning the formation of chemical waves, and new realistic models to describe these phenomena are developed. It becomes possible to study catalysis on an atomic level, which is necessary for the understanding of the mechanism of action of the high-dispersed supported metal catalysts having metal nanocrystallites 100–300 Å in size as active part of the catalyst. This result will open new fields for the development of theoretical concepts of heterogeneous catalysis. The most exciting result of this work lies in the following: the appearance of regular waves is an amazing example of self-organization of a catalytic reaction on a metal particle with a size of some hundreds angstrom.

Acknowledgement

This work is supported in part by RFBR Grant No. 05-03-32971 and NWO grant No. 047-015-002.

References

[1] G. Nicolis, I. Prigogine, Self-Organization in Nonequilibrium Systems, Wiley, New York, 1977.
[2] G. Ertl, Adv. Catal. 37 (1990) 213.
[3] R. Imbihl, Prog. Surf. Sci. 44 (1993) 185.
[4] R. Imbihl, G. Ertl, Chem. Rev. 95 (1995) 697.
[5] M.M. Slinko, N.I. Jaeger, Stud. Surf. Sci. Catal. 86 (1994) 1.
[6] C.A. de Wolf, B.E. Nieuwenhuys, Catal. Today 70 (2001) 287.
[7] K.C. Taylor, Catal. Rev. Sci. Eng. 35 (1993) 457.
[8] M.F.H. van Tol, A. Gielbert, B.E. Nieuwenhuys, Catal. Lett. 16 (1992) 297.
[9] V. Gorodetskii, J.H. Block, W. Drachsel, M. Ehsasi, Appl. Surf. Sci. 67 (1993) 198.

[10] M.P. Cox, G. Ertl, R. Imbihl, Phys. Rev. Lett. 54 (1985) 1725.
[11] M. Eiswirth, G. Ertl, Surf. Sci. 177 (1986) 90.
[12] M. Ehsasi, S. Rezaie-Serej, J.H. Block, K. Christmann, J. Chem. Phys. 92 (1990) 7596.
[13] H.-H. Rotermund, W. Engel, M. Kordesch, G. Ertl, Nature 343 (1990) 355.
[14] M. Ehsasi, A. Karpowichz, M. Berdau, W. Engel, K. Christmann, J.H. Block, Ultramicroscopy 49 (1993) 318.
[15] K.C. Rose, R. Imbihl, B. Rausenberger, C.S. Rastomjee, W. Engel, A.M. Bradshaw, Surf. Sci. 352–354 (1996) 258.
[16] V. Gorodetskii, W. Drachsel, J.H. Block, Catal. Lett. 19 (1993) 223.
[17] V. Gorodetskii, J. Lauterbach, H.-H. Rotermund, J.H. Block, G. Ertl, Nature 370 (1994) 276.
[18] V.V. Gorodetskii, W. Drachsel, Appl. Catal. A Gen. 188 (1999) 267.
[19] V. Gorodetskii, W. Drachsel, M. Ehsasi, J.H. Block, J. Chem. Phys. 100 (1994) 6915.
[20] V. Gorodetskii, W. Drachsel, J.H. Block, Appl. Surf. Sci. 76–77 (1994) 122.
[21] V.V. Gorodetskii, A.V. Matveev, A.V. Kalinkin, B.E. Nieuwenhuys, Chem. Sustain. Dev. 11 (2003) 67.
[22] T.V. de Bocarmé, N. Kruze, Topic Catal. 14 (2001) 35.
[23] P.D. Cobden, N.M.H. Janssen, Y. van Breugel, B.E. Nieuwenhuys, Faraday Disc. Chem. Soc. 105 (1996) 57.
[24] C. Voss, N. Kruse, Appl. Surf. Sci. 87–88 (1994) 127.
[25] P.D. Cobden, Y. van Breugel, B.E. Nieuwenhuys, Surf. Sci. 402–404 (1998) 155.
[26] P.D. Cobden, C.A. de Wolf, M.Yu. Smirnov, A. Makeev, B.E. Nieuwenhuys, J. Mol. Catal. A 158 (2000) 115.
[27] M.F.H. van Tol, P.T. Wouda, B.E. Nieuwenhuys, J. Vac. Sci. Techol. A 12 (1994) 2176.
[28] M.F.H. van Tol, Ph.D. Thesis, Leiden University, The Netherlands, 1993.
[29] A.R. Cholach, M.F.H. van Tol, B.E. Nieuwenhuys, Surf. Sci. 320 (1994) 281.
[30] M.F.H. van Tol, J. de Maaijer-Gielbert, B.E. Nieuwenhuys, Chem. Phys. Lett. 205 (1993) 207.
[31] V.I. Elokhin, E.I. Latkin, A.V. Matveev, V.V. Gorodetskii, Kinet. Catal. 44 (2003) 692.
[32] E.W. Müller, T.T. Tsong, Field Ion Microscopy, Elsevier, New York, 1969.
[33] P.D. Cobden, V.V. Gorodetskii, B.E. Nieuwenhuys, Surf. Sci. 432 (1999) 61.
[34] M.F.H. van Tol, F.A. Hondsmerk, J.W. Bakker, B.E. Nieuwenhuys, Surf. Sci. 266 (1992) 214.
[35] M.F.H. van Tol, F.A. Hondsmerk, J.W. Bakker, B.E. Nieuwenhuys, Surf. Sci. 266 (1992) 529.
[36] P.D. Cobden, B.E. Nieuwenhuys, V.V. Gorodetskii, Appl. Catal. A Gen. 188 (1999) 69.
[37] Yu. Suchorski, R. Imbihl, V.K. Medvedev, Surf. Sci. 401 (1998) 392.
[38] W. Drachsel, C. Wesseling, V. Gorodetskii, J. Phys. IV 6 (1996) 31.
[39] N. Ernst, G. Bozdech, V. Gorodetskii, J.H. Block, Mass Spectr. Ion Process. 152 (1996) 185.
[40] R.H. Fowler, L.W. Nordheim, Proc. R. Soc. (Lond.) A 119 (1928) 173.
[41] R.M. Wolf, J.W. Bakker, B.E. Nieuwenhuys, Surf. Sci. 246 (1991) 135.
[42] V. Gorodetskii, W. Drachsel, J.H. Block, J. Chem. Phys. 100 (1994) 6907.
[43] H.J. Kreuzer, R.L.C. Wang, Z. Phys. Chem. 202 (1997) 127.
[44] V. Gorodetskii, J.H. Block, W. Drachsel, Appl. Surf. Sci. 76–77 (1994) 129.
[45] V.P. Zhdanov, B. Kasemo, Surf. Sci. Rep. 20 (1994) 113.
[46] B. Sieben, G. Bozdech, N. Ernst, J.H. Block, Surf. Sci. 352–354 (1996) 167.
[47] J.H. Block, D.L. Cocke, N. Kruse, in: G. Ertl, H. Knözinger, J. Weitkamp (Eds.), Handbook of Heterogeneous Catalysis, vol. 3, Wiley, VCH, Weinheim (Germany), 1997, p. 1104.
[48] Y.-S. Lim, M. Berdau, M. Naschitzki, M. Ehsasi, J.H. Block, J. Catal. 149 (1994) 292.
[49] B. Sieben, Yu. Suchorski, G. Bozdech, N. Ernst, Z. Phys. Chem. 202 (1997) 103.
[50] M. Eiswirth, R. Schwankner, G. Ertl, Z. Phys. Chem. 144 (1985) 59.
[51] G. Ertl, P.R. Norton, J. Rüstig, Phys. Rev. Lett. 42 (1982) 177.
[52] H.H. Rotermund, S. Jakubith, A. von Oertzen, G. Ertl, Phys. Rev. Lett. 66 (1991) 3083.
[53] J. Lauterbach, H.H. Rotermund, Surf. Sci. 311 (1994) 231.
[54] E.I. Latkin, V.I. Elokhin, V.V. Gorodetskii, J. Mol. Catal. A 166 (2001) 23.
[55] R. Imbihl, M.P. Cox, G. Ertl, H. Müller, W. Brenig, J. Chem. Phys. 83 (1985) 1578.
[56] A. Hopkinson, X.-C. Guo, J.M. Bradley, D.A. King, J. Chem. Phys. 99 (1993) 8262.
[57] M. Gruyters, T. Ali, D.A. King, J. Phys. Chem. 100 (1996) 14417.
[58] V.V. Gorodetskii, A.V. Matveev, P.D. Cobden, B.E. Nieuwenhuys, J. Mol. Catal. A 158 (2000) 155.
[59] S. Ladas, R. Imbihl, G. Ertl, Surf. Sci. 280 (1993) 42.
[60] A.V. Matveev, E.I. Latkin, V.I. Elokhin, V.V. Gorodetskii, Chem. Eng. J. 107 (2005) 181.
[61] E.I. Latkin, V.I. Elokhin, A.V. Matveev, V.V. Gorodetskii, J. Mol. Catal. A 158 (2000) 161.
[62] E.I. Latkin, V.I. Elokhin, V.V. Gorodetskii, Chem. Eng. J. 91 (2003) 123.
[63] A.V. Matveev, E.I. Latkin, V.I. Elokhin, V.V. Gorodetskii, Chem. Sustain. Dev. 11 (2003) 173.
[64] B.C. Sales, J.E. Turner, M.B. Maple, Surf. Sci. 114 (1982) 381.
[65] V.P. Zhdanov, Surf. Sci. Rep. 45 (2002) 231.
[66] J.H. Block, M. Ehsasi, V. Gorodetskii, A. Karpowicz, M. Berdau, in: T. Inui, et al. (Eds.), New Aspects of Spillover Effect in Catalysis: Studies in Surface Science and Catalysis, vol. 77, Elsevier Science Publ. B.V., 1993, p. 189.
[67] A. Schaak, B. Nieuwenhuys, R. Imbihl, Surf. Sci. 441 (1999) 33.
[68] A. Schaak, R. Imbihl, J. Chem. Phys. 113 (2000) 9822.
[69] E. Schütz, F. Esch, S. Günther, A. Schaak, M. Marsi, M. Kiskinova, R. Imbihl, Catal. Lett. 63 (1999) 13.
[70] V.V. Gorodetskii, V.A. Sobyanin, N.N. Bulgakov, Z. Knor, Surf. Sci. 82 (1979) 120.
[71] V.V. Gorodetskii, B.E. Nieuwenhuys, W.M.H. Sachtler, G.K. Boreskov, Appl. Surf. Sci. 7 (1981) 355.
[72] J. Wintterlin, Adv. Catal. 45 (2000) 131.
[73] J.H. Block, V.V. Gorodetskii, W. Drachsel, Recl. Trav. Chim. Pays-Bas 113 (1994) 444.
[74] K. Heiz, E. Lang, K. Strauss, K. Müller, Appl. Surf. Sci. 11–12 (1982) 611.
[75] V.P. Zhdanov, B. Kasemo, Surf. Sci. 496 (2002) 251.
[76] V.P. Zhdanov, Catal. Lett. 93 (2004) 135.
[77] D.Yu. Zemlyanov, M.Yu. Smirnov, V.V. Gorodetskii, Catal. Lett. 43 (1997) 181.
[78] Ch. Romainczyk, J.R. Manson, K. Kern, K. Kuhnke, R. David, P. Zeppenfeld, G. Gomsa, Surf. Sci. 336 (1995) 362.
[79] J.L. Gland, M.R. McClellan, F.R. McFeely, J. Chem. Phys. 79 (1983) 6349.
[80] B.E. Nieuwenhuys, Adv. Catal. 44 (1999) 259.
[81] M.F.H. van Tol, A. Gielbert, B.E. Nieuwenhuys, Appl. Surf. Sci. 67 (1993) 179.
[82] S. Heinze, V. Schmatloch, N. Kruze, Surf. Sci. 341 (1995) 124.
[83] H. Hirano, T. Yamada, K.I. Tanaka, J. Siera, B.E. Nieuwenhuys, Surf. Sci. 262 (1992) 97.
[84] H. Hirano, T. Yamada, K.I. Tanaka, J. Siera, B.E. Nieuwenhuys, in: L. Guczi, et al. (Eds.), Proceedings of the 10th ICC, Budapest, New Frontiers in Catalysis, Akademiai Kiado, Budapest, 1993, p. 347.
[85] F. Mertens, R. Imbihl, Surf. Sci. 347 (1996) 355.
[86] N.M.H. Janssen, B.E. Nieuwenhuys, M. Ikai, K. Tanaka, A.R. Cholach, Surf. Sci. 319 (1994) L29.

[87] A. Schaak, S. Günther, F. Esch, E. Schütz, M. Hinz, M. Marsi, M. Kiskinova, R. Imbihl, Phys. Rev. Lett. 83 (1999) 1882.
[88] A.G. Makeev, M.M. Slinko, N.M.H. Janssen, P.D. Cobden, B. Nieuwenhuys, J. Chem. Phys. 105 (1996) 7210.
[89] M.Yu. Smirnov, V.V. Gorodetskii, A.R. Cholach, in: H.H. Brongersma, R.A. van Santen (Eds.), Fundamental Aspects of Heterogeneous Catalysis Studied by Particles Beams, Plenum Press, New York, 1991, p. 249.
[90] D.Yu. Zemlyanov, M.Yu. Smirnov, V.V. Gorodetskii, J.H. Block, Surf. Sci. 329 (1995) 61.
[91] D.Yu. Zemlyanov, M.Yu. Smirnov, V.V. Gorodetskii, Surf. Sci. 391 (1997) 37.
[92] M. Slinko, T. Fink, T. Löher, H.H. Madden, S.J. Lombardo, R. Imbihl, G. Ertl, Surf. Sci. 264 (1992) 157.
[93] S.J. Lombardo, M. Slinko, T. Fink, T. Löher, H.H. Madden, F. Esch, R. Imbihl, G. Ertl, Surf. Sci. 269–270 (1992) 481.
[94] J. Siera, P. Cobden, K. Tanaka, B. Nieuwenhuys, Catal. Lett. 10 (1991) 335.
[95] M.F.H. van Tol, J. Siera, P. Cobden, B. Nieuwenhuys, Surf. Sci. 274 (1992) 63.
[96] H.H. Madden, R. Imbihl, Appl. Surf. Sci. 48–49 (1991) 130.
[97] P.D. Cobden, J. Siera, B.N. Nieuwenhuys, J. Vac. Sci. Technol. A 10 (1992) 2487.
[98] B. Rausenberger, M. Mundschau, W. Swiech, W. Engel, A.M. Bradshaw, J. Chem. Soc. Faraday Trans. 92 (1996) 4815.
[99] A.G. Makeev, B.E. Nieuwenhuys, J. Chem. Phys. 108 (1998) 3740.
[100] A.G. Makeev, B.E. Nieuwenhuys, Surf. Sci. 418 (1998) 432.
[101] Yu. Suchorski, J. Beben, R. Imbihl, Prog. Surf. Sci. 59 (1998) 343.
[102] Yu. Suchorski, J. Beben, R. Imbihl, Surf. Sci. 454-456 (2000) 331.
[103] Yu. Suchorski, J. Beben, R. Imbihl, E.W. James, L. Da-Jiang, J.W. Evans, Phys. Rev. B 63 (2001) 165417.
[104] G.A. Somorjai, Adv. Catal. 26 (1977) 2.
[105] G. Ertl, Adv. Catal. 45 (2000) 1.